Modelling the long-term dynamics and inhibitory effects of crude glycerol impurities in a methanogenic and sulfidogenic UASB bioreactor

Eric Valdés [a], David Gabriel [a], Daniel González [a], Giulio Munz [b]

[a] GENOCOV Research group, Department of Chemical, Biological and Environmental Engineering, Escola d'Enginyeria, Universitat Autònoma de Barcelona, 08193 Bellaterra, Spain

[b] Department of Civil and Environmental Engineering, University of Florence, Via di S. Marta, 3, 50139, Firenze, Italy

* Corresponding author.

E-mail address: David.Gabriel@uab.cat (D. Gabriel)

Full postal address: Escola d'Enginyeria, Universitat Autònoma de Barcelona, 08193 Bellaterra, Spain

Abstract

The performance of Upflow Anaerobic Sludge Blanket (UASB) bioreactors treating sulfate (SO_4^{2-}) -rich effluents depends on multiple factors, including microbial interactions and operational conditions. The high complexity of these systems necessitates the use of mathematical modelling tools to better understand the process and predict the long-term impacts of various operational variables. In this work, a mathematical model describing the long-term operation of a sulfate-fed 2.5L UASB reactor was developed, calibrated and validated. Crude glycerol was used as electron donor to achieve sulfate reduction. The hydraulic model of the UASB was described as a set of CSTRs in series to represent its plug flow-like behavior. The kinetic model included 8 fermentation processes using glycerol as the primary electron source, 5 sulfate-reduction processes using organic and inorganic electron sources, and 2 methanogenic processes. The model tackled the long-term accumulation of the impurities coming from the crude glycerol solution, namely slime -like-substances (SLS), and their inhibitory effects over the three different trophic groups: fermenters, sulfate-reducers and methanogens. A sensitivity analysis and calibration of the most relevant parameters was performed using the experimental data from 280 days of continuous operation of a lab-scale UASB. Volatile suspended solids (VSS), carbon (C) and sulfur (S) species profiles as well as microbial dynamics from initial methanogenic conditions to non-methanogenic conditions due to SLS impact were properly predicted by the model under steady-state feeding conditions. Furthermore, the model was validated using another independent set of data under dynamic-feeding conditions, containing 6 different phases with varying HRT, inlet sulfate and organic carbon concentrations. After successfully validating the model, a scenario analysis was conducted to evaluate two case studies, with different inlet sources: crude glycerol with varying SLS concentrations and pure glycerine (SLS-free). The results of the simulations suggest that heterotrophic SR have greater long-term resistance to the inhibitory effects of SLS, compared to methanogens. Methane production increased with higher C and S loading rates, and the balance between sulfate reduction efficiency and COD removal was optimal at a C/S ratio of 1.6 g C g S^{-1}.

Keywords: Upflow Anaerobic Sludge Blanket (UASB); sulfate reduction (SR); methanogenesis inhibition; mathematical modelling; model calibration; model validation.

1. Introduction

Sulfur dioxide (SO_2) is a colorless gas that leads to the formation of acid rain, which can negatively impact the environment; it causes deforestation, acidifies waterways and is corrosive to building materials and paints. Moreover, it is highly odorous and can be harmful to human health under high exposure times. Approximately 70% of SO_2 in the atmosphere is originated by anthropogenic activity (Smith et al., 2001), coming mostly from the oxidation of sulfur– containing matter during heating and combustion processes. Thus, different control methods have been implemented during the last decades which have led to a global decrease in SO_2 emissions (Chen et al., 2021). While the most common technologies to capture SO_2 – such as wet flue gas desulfurization, WFGD – can effectively reduce the emissions, they often come with high costs and generate alkaline, S-rich effluents that must be treated before being released into the environment. Biological processes offer a more sustainable and cost-effective alternative to traditional chemical and physical methods; these processes do not rely on the use of strong chemicals, resulting in fewer harmful by-products and waste. Additionally, the circular economy – driven nature of such processes can lead to reduce the operational costs, making them a financially viable option.

The SONOVA – Sulfur Oxide, Nitrogen Oxide VAlorisation – process proposed by (Mora et al., 2020) integrates the principles of bioeconomy and targets the treatment of SOx-rich flue gases for biosulfur recovery. This two-stage bioscrubber consists first of an absorption unit using a slightly alkaline solution to absorb the SO_2, and a two-step biological treatment of the sulfite/sulfate- rich absorbate consisting of the reduction to sulfide in a UASB reactor and the subsequent partial oxidation to elemental sulfur under microaerophilic conditions in a Continuous Stirred Tank Reactor (CSTR) (see figure S4). The initial study of the individual stages of the process revealed promising results, showing high efficiency in the physical absorption and biological treatment units.

With the aim of exploring the possible limitations of the first biological stage of the SONOVA process, (Fernández-Palacios et al., 2019) studied the operational limits of a sulfidogenic UASB reactor fed with sulfate utilizing crude glycerol as the carbon and electron source. The maximum elimination capacity of sulfate was 4.3 kg $S\text{-}SO_4^{2-}$ L^{-1} h^{-1} at a COD/S ratio of 5.4 g O_2 g S^{-1}. The methanogenic activity ceased after 200 days of operation which led to the accumulation of volatile fatty acids (VFA), mainly acetate and propionate. Likewise,

similar results were reported by (Zhou et al., 2024), where methane production also started shrinking after 100 days of operation; microbial diversity analyses revealed the complete washout of methanogens after 230 days of operation. Moreover, the authors reported the formation and accumulation of slime-like substances (SLS), which could have contributed to the collapse of the experimental system. Further analysis of the slime-like biofilm attached to the granules revealed a high concentration of long-chain fatty acids (LCFAs), particularly palmitic acid. These compounds represent a fraction of the many impurities contained in the crude glycerol generated from both plant seed oils and used cooking oils in the biodiesel industry (Hu et al., 2012). Some studies have analyzed the content of LCFAs in crude glycerol, reporting concentrations ranging from 0.48% to 2.5% in w/w (J. Chen et al., 2018; Viana et al., 2012). Furthermore, they have been shown to inhibit biomass growth when compared to purified glycerol (J. Chen et al., 2018). Likewise, several studies have shown that LCFAs can inhibit methanogenesis (Deaver et al., 2020; Wu et al., 2017; Pereira et al., 2005;Dasa et al., 2016;Koster & Cramert, 1987; Silva et al., 2016).According to the Anaerobic Digestion Model number 1 (Batstone et al., 2002) there are three main mechanisms by which LCFAs can inhibit methanogenesis: competitive inhibition, electron transport chain uncoupling and mass transfer limitation caused by adhesion to the bacterial cell wall. Therefore, the attachment of SLS onto the granule surface could have plausibly hindered methanogenesis by limiting mass transfer of the substrate.

In recent years, the development and application of mathematical models has become increasingly pivotal in the field of UASB bioreactors; mathematical models can be a powerful tool to predict the dynamic behavior of these very complex systems. As such, they have emerged as suitable tools to optimize the design, operation, and control of these processes. In this field, the ADM1 laid the groundwork of a comprehensive model for the anaerobic digestion process with a strong focus on the biochemical conversion of organic C. It described the disintegration and hydrolysis of complex structures into soluble and bioavailable compounds, the acidogenesis of sugars and amino acids into VFAs, the acetogenesis of VFAs and ultimately the methanization processes; nonetheless, it focused solely on biochemical pathways. Thus, many authors have dedicated efforts on describing the hydraulic behavior of UASB bioreactors (Y. Chen et al., 2015; Zeng et al., 2005). Moreover, given the exclusion of sulfate-reduction from ADM1, there has also been a notable surge in research aimed at expanding the model incorporating this process. In these newly developed models, hydrogen and acetate are generally regarded as the main electron donors for sulfate- reduction processes, carried out by autotrophic and

heterotrophic sulfate-reducing bacteria (ASRB and HSRB, respectively); (Barrera et al., 2015) added propionate, (Flores-Alsina et al., 2016) also included butyrate and valerate and (Wang et al., 2021) proposed ethanol as an alternate source of electrons. Following the above-mentioned work (Zhou et al., 2024) on the operation of the sulfidogenic UASB, (Zhou, Fernández-Palacios, et al., 2022) performed an in-depth study on the mechanisms behind sulfate-reduction using glycerol fermentation products as the electron source and concluded that ethanol, propionate, formate and 1,3- propanediol were the main organic compounds involved. The proposed kinetic model with these new biochemical pathways paved the way to model the sulfate-reducing UASB of the SONOVA bioscrubber.

In this study, the UASB reactor with sulfate reduction using glycerol as an external carbon source was modeled with a special focus on SLS accumulation and its effects on the long-term dynamics of VSS, C and S species. The model incorporates glycerol fermentation, sulfate-reduction and methanogenic processes and tackles the competition between different trophic groups. While the over-competition of sulfate-reducing bacteria over methanogens has been widely reported in the literature (Jing et al., 2013; J. Wu et al., 2018; Li et al., 2023) and even modelled (Fedorovich & Kalyuzhnyi, 1997; Sun et al., 2016; ; H. Chen et al., 2019; Wang et al., 2021), no study has mathematically described this phenomenon by means of the mass-transfer limitations caused by the accumulation of impurities – namely SLS – inside the reactor. The model was calibrated using the experimental data from the operation of (Zhou et al., 2024) under steady- state feeding conditions, and validated using the data from (Fernández-Palacios et al., 2019), with dynamic feeding conditions. Finally, the model was used to predict the potential impact of different scenarios on biomass dynamics, sulfate and COD removal and methane production.

2. Methodology

2.1.Description of the modelled system

The model aims to describe the main hydraulic and kinetic processes that took place inside the UASB reactor carried out by (Zhou et al., 2024) during the transition between methanogenic to non-methanogenic condition. This reactor was inoculated with granular sludge from a full-scale anaerobic UASB digester from a pulp and paper recycling industry; microbial diversity analyses of the inoculum showed the predominance of methanogenic populations over sulfidogenic.

This system targeted the biological reduction of sulfate into sulfide using crude glycerol as an external source of carbon; glycerol fermentation can produce a mixture of VFAs and alcohols that serve as electron donors for SR bacteria. Additionally, methane was produced by methanogenic populations, potentially through both the acetoclastic – using acetate – and hydrogenotrophic – using H_2 and CO_2 – pathways.

The mechanistic model for the glycerol fermentation and sulfate reduction processes was studied (Zhou, Fernández-Palacios, et al., 2022), and concluded that glycerol fermentation produced five main intermediates, four of which - ethanol, 1,3-propanediol, formate and propionate – provided the electrons for SR processes. The remaining intermediate, 3-hydroxypropionate, was mainly oxidized to acetate.

The 2.5 L bioreactor was run for 639 days under pseudo steady-state feeding conditions with an inlet sulfate concentration of 250 mg S L^{-1} and keeping a C/S ratio around 1.5 g C g S^{-1}. The reactor consisted of a cylindrical vessel with a diameter of 5.6 cm and a height of 1 m, equipped with sampling points located at 7 cm, 28 cm, and 72 cm along the height of the reactor to monitor the VSS.As reported by the authors, the accumulation of a slime-like substance (SLS) originating from the glycerol solution was observed throughout the operation of the reactor; the consequent attachment of this substance onto the surface of the granules and the walls of the reactor led to a decrease of methane production and removal efficiencies. To incorporate these phenomena into the model, the SLS fraction of the TOC from the inlet solution was calibrated using the granule composition analysis from (Zhou et al., 2024). Since the proper description of SLS accumulation and VSS dynamics was considered crucial for the modelling goals of this work, the calibration of critical parameters to accurately represent the solids of the system at different heights was done prior to model calibration, as will be explained in the following

144 section. To this aim, samples taken at 3 different heights – 7, 28 and 72 cm from the reactor bottom; ports 1,3
145 and 6 respectively – were used to assess solids concentrations.
146 After day 280 of operation, no methane was detected in the outlet gas stream, and both sulfate and glycerol
147 removal efficiencies began to decline. It should be noted that the subsequent collapse of the system, specifically
148 regarding the loss of glycerol fermentation, is beyond the scope of this study; for this reason, only the first three
149 stages of operation were considered for modelling purposes (days 0-280).
150
151 *2.2.Model assumptions*
152 During the process of model development process some important assumptions were made to effectively
153 describe the main phenomena, while simultaneously prioritizing the simplicity of the model.
154 i) First, based on visual observations from the system and the VSS measurements reported (Zhou et al.,
155 2024), the UASB reactor was discretized in a set of 3 mini-CSTRs – vertical layers – in series; this simplification
156 to represent the plug flow – like behaviour of the system has been previously used by other authors (Boiocchi
157 et al., 2022; Nugroho & Santoso, 2019;Rodríguez-Gómez et al., 2014). The mass balances for all the species
158 considered in the system were solved following Eq. 1:
159

$$\frac{dS_n}{dt} = \frac{F_{in} \cdot w}{V_i} \cdot (S_{n-1} - S_n) + R_n \qquad \text{Eq. (1)}$$

160
161 Where F_{in} is the inlet flowrate [L d^{-1}], V_i is the volume of mini-CSTR *i,* S_{i-1} and S_i are the inlet and outlet
162 concentrations of component S in reactor *i,* and r_i is the conversion rate of *S* in reactor *n* [mg S L^{-1} d^{-1}]. A
163 washout factor *w* was considered for the solid components (active biomass, inert solids and SLS) in the two
164 bottom CSTRs to simulate their transport dynamics along the height of the reactor; for the soluble compounds
165 *w* was equal to 1 throughout the whole reactor. This type of variable has been implemented before to simulate
166 VSS dynamics in discretized UASB (Nugroho & Santoso, 2019); analogously, (Boiocchi et al., 2022) used a
167 dragging coefficient (k_{drag}) representing the volume of solids dragged per volume unit of methane produced.
168 ii) The kinetic model is based on the ADM1 with additional processes accounting for glycerol fermentation
169 and SR, which had been studied and mechanistically determined by (Zhou, Dorado, et al., 2022). The model

170 considers 5 biomass trophic groups (fermentative bacteria X_{FB}; heterotrophic and autotrophic sulfate reducers,
171 X_{HSRB} and X_{ASRB}; hydrogenotrophic and acetoclastic methanogens, X_{HM} and X_{AM}) which carry out 15 biochemical
172 processes: glycerol fermentation and acidogenesis of fermentation products (8), heterotrophic SR (4),
173 autotrophic SR (1), hydrogenotrophic methanogenesis (1) and acetoclastic methanogenesis (1). All these
174 reactions are rate-controlled (i.e., there are no mass transfer limitations), and the consumption rates followed a
175 Monod – type kinetic rate equation.
176 iii) Biomass decay was considered for all five trophic groups as they are considered to constitute granules
177 inside the reactor. The decay product, namely composites, was assumed to be a mixture of non-degradable inert
178 solids and degradable soluble carbohydrates which can be hydrolyzed into bioavailable substrate – glycerol in
179 this model.
180 iv) Free sulfide inhibition on sulfate- reduction processes was considered by means of a non-competitive
181 inhibition term as described in (Batstone & Keller, 2003)
182 v) Inhibition caused by SLS accumulation was accounted by means of a modified version of the non-
183 competitive inhibition term reported by (Ma et al., 2015) (Eq 2):
184

$$I_{SLS,k} = \frac{ki_{SLS,k}\frac{X_k}{X_{SLS}}}{ki_{SLS,k}\frac{X_k}{X_{SLS}} + X_{SLS}} \qquad \text{Eq. (2)}$$

185 Where $ki_{SLS,k}$ is the inhibition constant of SLS over trophic group k [mg COD_{SLS} L^{-1}] and X_{SLS} is the
186 concentration of SLS [mg COD_{SLS} L^{-1}].
187 vi) Liquid-gas transfer processes were also taken into account as had been reported in ADM1 and other
188 works (Rosén et al., 2006). The gas flowrate was calculated considering the sum of the partial pressures times
189 the total gas flow rate of hydrogen H_2 [mg H2 d^{-1}], carbon dioxide CO_2 [mg C d^{-1}], hydrogen sulfide H_2S [mg S
190 d^{-1}] and methane CH_4 [mg C d^{-1}]. An over-pressure in the headspace was assumed to calculate the gas flowrate,
191 as described in (Rosén et al., 2006), considering the headspace as a vessel of volume equal to 10% of the mini-
192 CSTR at the top of the reactor. Henry's law was considered to calculate liquid-gas mass transfer.
193 vii) The pH was calculated by means of an algebraic equation as described in the report by (Rosén et al.,
194 2006).

To have a more in-depth understanding about how the model is formulated, the authors refer to Supplementary Material, section I (mathematical model formulation).

2.3.Pre-calibration, calibration and validation of the model

In order to calibrate and validate the model, a multi-step procedure was implemented, consisting of model pre-calibration, sensitivity analysis, model calibration, identifiability analysis and model validation. Prior to model validation, the dataset from Zhou et al. (2024), in which the UASB was run under pseudo-steady state feeding conditions, was utilized. Each one of the steps will be detailed in this section.

Model pre-calibration

Since the established configuration of the model was extremely sensitive to the solid compounds' dynamics, which were strongly affecting SLS inhibition (see Eq 4), a model pre-calibration of the parameters dictating the VSS was performed prior to sensitivity analysis. The selected parameters were the biomass maximum specific decay rate k_d [d^{-1}], the washout constant w [-] and the SLS fraction of the inlet TOC solution f_{SLS} [-]. This selection was made based on the authors' knowledge and expertise, considering the established influence of these parameters on VSS dynamics. This pre-calibration procedure was implemented with the *fminsearch* (Nelder-Mead algorithm, Simplex) command featured in MATLAB® 2021b, which searches for the minimum of a given function returning a set of optimized variables of said function. The objective function F was defined as the sum of the norm of the differences between the experimental values of VSS at ports 1 and 3 and the model predictions at mini-CSTRs 1 and 2, respectively (Eq 3).

$$F = \sqrt{\left(\sum_{i=1}^{n}[VSS_{exp1,i} - VSS_{mod1,i}]^2 + \sum_{i=1}^{n}\left[VSS_{exp3,i} - VSS_{mod2,i}\right]^2\right) \cdot \frac{1}{n} + [SLS_{fit}]^2} \quad \text{Eq. (3)}$$

Where n is the number of experimental values, and SLS_{fit} is defined as:

$$SLS_{fit} = VSS_{mod1,315.} \cdot 0.48 - SLS_{mod1,315} \quad \text{Eq. (4)}$$

Implying that the predicted value of the SLS should be equal to 48% of the predicted VSS on day 315 of simulation, at the bottom of the reactor, as the findings by (Zhou et al., 2024) suggested.

Model calibration

After model pre-calibration, a sensitivity analysis was performed to find the most relevant parameters for model calibration. The equations and procedure followed during sensitivity analysis can be found in the SM (section II).

After performing the sensitivity analysis, the 6 most sensitive parameters (i.e., the parameters with the highest relative sensitivities) were selected for calibration. The objective function F considered the following model outputs: acetate, propionate and total inorganic carbon (TIC) outlet concentrations [mg C L^{-1}] and methane outlet mass flowrate [mg C d^{-1}] (Eq 5).

$$F = \sqrt{\sum_{j=1}^{m} \sum_{i=1}^{n} [y_{exp,j,i} - y_{mod,j,i}]^2} \quad \text{Eq. (5)}$$

Where m is the number of output variables, n is the number of experimental data, y_{exp} is the experimental value and y_{mod} is the predicted value.

The goodness of fit was quantitatively assessed through the Theil Inequality Coefficient (ThIC), which was calculated according to Equation 6 (Xianmin, 1993):

$$ThIC = \frac{\sqrt{\sum_{i}^{m} (y_{exp,i} - y_{mod,i})^2}}{\sqrt{\sum_{i}^{m} y_{exp,i}{}^2} + \sqrt{\sum_{i}^{m} y_{mod,i}{}^2}} \quad \text{Eq. (6)}$$

ThIC values range between 0 and 1, being 0 a model output with no differences with the experimental data (i.e., a model with no errors in its predictions) and 1 the limit value when differences tend to be infinite. It is generally accepted to consider a maximum ThIC of 0.3 as the threshold for a good fit of the modeling results (Xianmin, 1993), as other studies have employed this approach to compare mathematical models performance (Valdés et al., 2023; Huiliñir et al., 2010) and model validation (Huiliñir et al., 2010).

The calibrated values were then assessed using the Fisher Information Matrix (FIM), which summarizes the uncertainties and dependencies among the estimated parameters (Guisasola et al., 2006). This methodology takes into account the quantity and quality of the utilized data as well as the output sensitivity functions for each parameter and can be used to calculate the standard errors of each estimation.

Model validation

After parameter optimization, the model was validated using the experimental data from (Fernández-Palacios et al., 2019), in which a very similar setup was carried out for 400 days under dynamic feeding conditions – varying sulfate and organic loading rates through 6 different stages. The operational conditions are summarized in table 1.

Table 1. Operational conditions of the UASB reactor used for model validation (adapted from Fernández-Palacios et al., 2019).

Stage (days)	**Hydraulic retention time [h]**	**Inlet sulfate concentration [mg S-SO_4^{2-} L^{-1}]**	**Inlet TOC concentration [mg C-TOC L^{-1}]**
I (0-99)	1.8	232.6	285.3
II (99-115)	2.2	244.5	423.9
III (115-197)	2.3	442.3	753.2
IV (197-238)	2.2	444.3	830.5
V (238-288)	2.5	859.7	862.9
VI (288-400)	2	440	710.6

The same inhibition pattern caused by SLS accumulation was observed during that run; hence, the goal of model validation was to assess the reliability of the calibrated model to predict the transition dynamics of the reactor from methanogenic to non-methanogenic conditions using a different dataset. The validation performance was estimated using the root mean squared error (RMSE) between model predictions and experimental values (Eq 7):

$$RMSE = \sqrt{\sum_{j=1}^{m} \frac{1}{n} \cdot \sum_{i=1}^{n} [y_{exp,j,i} - y_{mod,j,i}]^2} \quad \text{Eq. (7)}$$

The available data for model validation included acetate and propionate outlet concentrations [mg C L^{-1}], sulfate and sulfide outlet concentrations [mg S L^{-1}], methane and CO_2 mass flowrates [mg C d^{-1}].

3. Results and discussion

3.1.Model pre-calibration

A proper understanding of the solids dynamics inside the reactor was key for the aim of this study. For this reason, model pre-calibration was performed first.

In this stage the main critical parameters were previously identified as the biomass maximum specific decay rate k_d [d^{-1}], the washout constant w [-] and the SLS fraction of the inlet TOC solution f_{SLS} [-]. The results after optimization of the objective function are shown in table 2:

Table 2. Estimated parameters and goodness-of-fit after model pre-calibration.

Parametric estimation			Goodness-of-fit	
Optimized parameter	**Default value**	**Calibrated value**	**Variable adjusted**	**ThIC**
μ_{dec} [d^{-1}]	[a]0.2	0.14	VSS at $CSTR_1$ [mg VSS L^{-1}]	0.05
w [-]	[b]$2 \cdot 10^{-4}$	$2.54 \cdot 10^{-4}$	VSS at $CSTR_2$ [mg VSS L^{-1}]	0.09
f_{SLS} [-]	0.01	0.0065		

[a] Default value taken from (Batstone & Keller, 2003).
[b] Default value taken from (Boiocchi et al., 2022).

The predicted outcomes of the VSS at ports 1 (H=7 cm) and 3 (H=28 cm) of the UASB – represented by mini-CSTRs 1 and 2, respectively, in the model –, as well as SLS accumulation profile, are shown in figure 1.

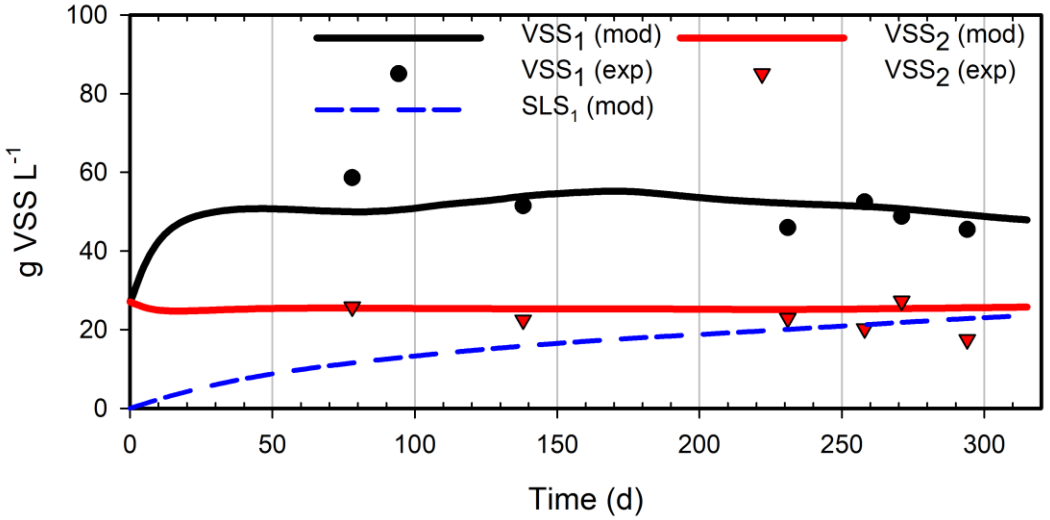

Fig. 1. Model pre-calibration outcomes. Lines represent the model predictions: total VSS at $CSTR_1$ (straight black) and $CSTR_2$ (straight red); SLS at $CSTR_1$ (dashed blue). Symbols represent the experimental values: total VSS at height H= 7 cm (black spheres) and H=28 cm (red triangles).

Port 3 was excluded from consideration as the washout coefficient was only applied to the particulate compounds at the two bottom CSTRs, as detailed in the model assumptions section, therefore these parameters were not sensitive to the simulated values at the top CSTR. As can be observed, the discretization of the UASB into mini-CSTRs allowed for a proper description of the VSS distribution along the height of the reactor. After parametric calibration, the model predictions described the VSS at 2 different heights with sufficient accuracy, as the obtained low ThIC values indicate (see table 2). Moreover, the resulting SLS accumulated after 315 days of operation represented roughly 50% of total VSS at the bottom of the reactor; these predicted values are in accordance with the experimental findings by (Zhou et al., 2024). The calibrated parameters show that the fraction of SLS coming from the glycerol solution was 0.65% in w/w, which falls within the range of 0.48% to 2.5% reported by other authors (J. Chen et al., 2018; Viana et al., 2012). A proper calibration of this parameter is crucial to implementing the developed mathematical model. Therefore, more precise measurements of impurities and detailed compositional analyses of the utilized crude glycerol solution could significantly improve the accuracy and reliability of the calibrated model.

3.2.Model calibration

After model pre-calibration, a sensitivity analysis was run to select the adequate parameters for model calibration; the results can be found in the supplementary material (table SM.1). In light of the obtained results and taking into account the authors' knowledge on the process and model, a set of 8 parameters was chosen for the calibration procedure; this selection was found critical to balance parametric identifiability and model accuracy. The parametric estimations after model calibration are shown in table 3, and the model predictions of 280 days of operation are shown in figure 2.

Table 3. Parametric estimation and goodness-of-fit assessment after model calibration.

Parametric estimation			**Goodness-of-fit**	
Optimized parameter	**Default value (units)**	**Calibrated value**	**Variable adjusted**	**ThIC**
km_{pro}	[a]9.96 [mg C mg VSS^{-1} h^{-1}]	4.24 (±0.17%)	Acetate outlet [mg C L^{-1}]	0.11
km_{am}	[b]1.23 [mg C mg VSS^{-1} h^{-1}]	0.74 (±0.02%)	Propionate outlet [mg C L^{-1}]	0.27
$km_{1-3,pd}$	[a]4.62 [mg C mg VSS^{-1} h^{-1}]	18.73 (±0.05%)	Methane outlet [mg C h^{-1}]	0.16
$km_{3hp,1}$	[a]2.56 [mg C mg VSS^{-1} h^{-1}]	0.06 (±4.22%)	TIC outlet [mg C h^{-1}]	0.11
$ki_{sls,m}$	[c]$5 \cdot 10^3$ [mg COD_{SLS} L^{-1}]	$2.14 \cdot 10^3$ ($\pm 2.2 \cdot 10^{-6}$ %)	Sulfate outlet [mg S L^{-1}]	0.18
$ki_{sls,sr}$	[c]$5 \cdot 10^3$ [mg COD_{SLS} L^{-1}]	$6.54 \cdot 10^3$ ($\pm 9.6 \cdot 10^{-6}$ %)	Sulfide outlet [mg S L^{-1}]	0.09
ks_{pro}	[d]79.00 [mg C L^{-1}]	53.43 (±0.02%)	[e]VSS at layer 1 [mg VSS L^{-1}]	0.04
ks_{am}	[b]47.85 [mg C L^{-1}]	1.01 (±0.47%)	[f]VSS at layer 2 [mg VSS L^{-1}]	0.06

[a] Default value taken from Zhou, Dorado, et al. (2022).

[b] Default value taken from Batstone & Keller (2003)

[c] Default value taken from Ma et al. (2015).

[d] Default value taken from Fedorovich & Kalyuzhnyi (1997).

[e-f] These two variables were not used for model calibration, but rather for model pre-calibration (see previous section); the resulting ThIC values are shown for informative purposes.

316 The goodness-of-fit of all the variables is also supported by the calculated ThIC values shown in table 3, all of
317 which fall below the threshold of 0.3 for all the selected adjusted variables.

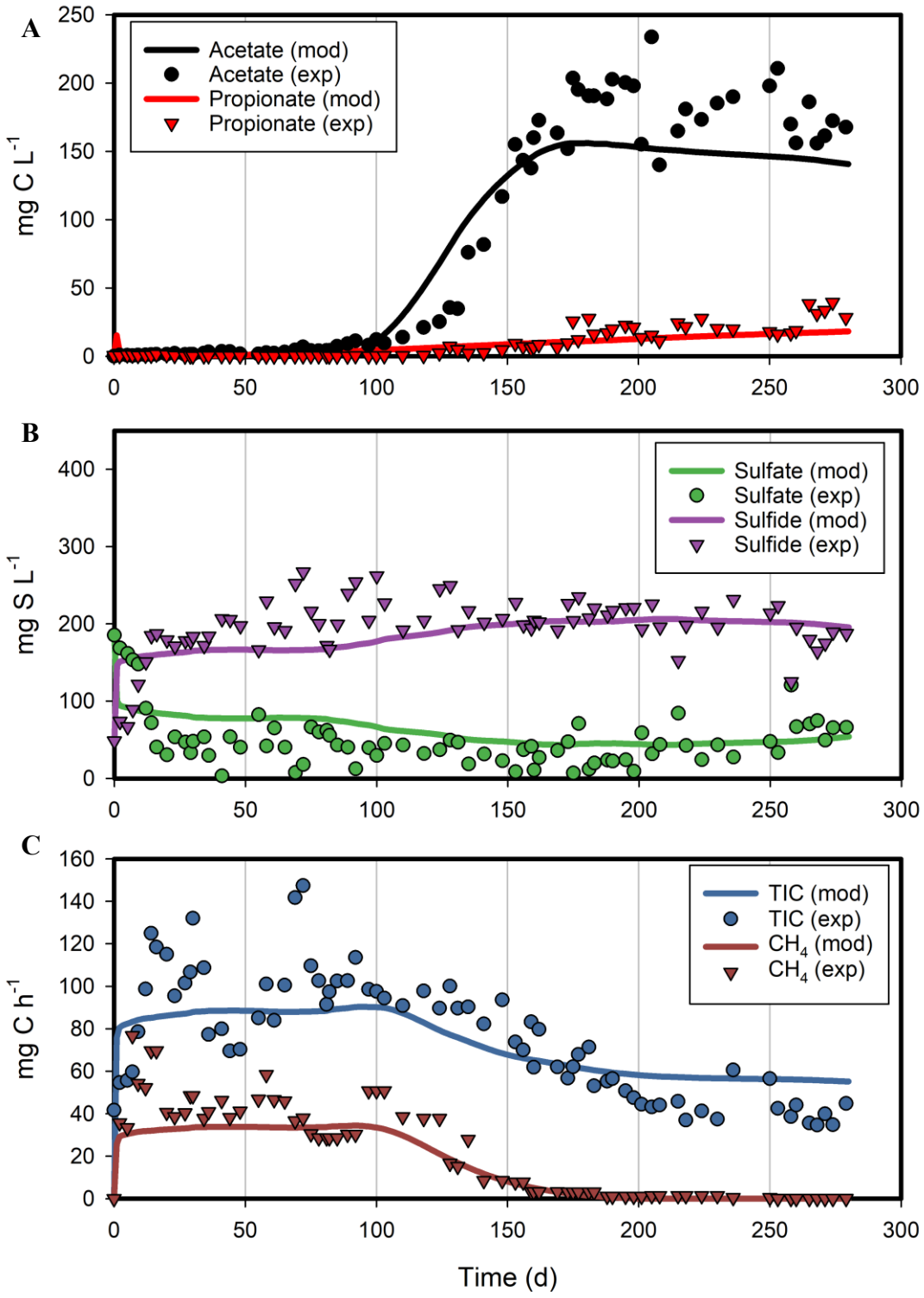

Fig. 2. Model calibration results of: (A) acetate and propionate outlet concentrations, (B) sulfide and sulfate outlet concentrations and (C) methane and TIC outlet mass flowrates.

Regarding the parametric estimations, the calibrated values are all in the same order of magnitude compared to the default values, except for $km_{3hp,1}$ - the maximum specific uptake rate of 3-hydroxypropionate by fermentative bacteria – which was estimated to a much lower value than that found by (Zhou, Dorado, et al., 2022): 0.06 to 3.17 mg C mg VSS^{-1} h^{-1}, respectively. This value depends on the specific activity of the fermentative bacteria present in the granules. Since the original batch tests to calibrate this parameter were conducted after 419 days of operation, it is possible that the microbial composition of the fermentative culture had changed, leading to different selective fermentative pathways. Nevertheless, all parameters have confidence intervals within 10% of their absolute values, attesting that the calibration was performed with high-quality data and appropriate parametric sensitivity.

As shown in figure 2, the model simulations were able to replicate the experimental data with good accuracy, particularly highlighting the transition between methanogenic and non- methanogenic conditions. The model also predicted the pH outcomes with good accuracy (see figure S1). However, the model's inability to capture the initial sludge adaptation phase to sulfidogenic conditions is evident in the sulfate and sulfide profiles; the dynamics of this initial step fell outside the scope of this study. Altogether, three different phases can be distinguished: biogas production (BP) phase, from 0-100 days, a transient phase from 100-230 days and a non-biogas production (NBP) phase from 230 to 280 days. The very same pattern is recognized if we look at the simulated biomass profiles (figure 3) and it can be explained due to the accumulation of SLS and its inhibitory effect on methanogenic populations (X_{AM} and X_{HM}). Such inhibition started taking place on day 100 at the bottom of the reactor, with a SLS concentration around 23 g COD L^{-1}. A more in-deep characterization of the SLS revealed the presence of fatty acid methyl esters (FAMEs) and free acids, with concentrations as high as 42% of the SLS dry weight in some samples (Fernández-Palacios, 2020). It has been reported by many studies that these types of compounds have detrimental effects on methanogenesis, with inhibitory ranges of 0.5-1.5 g COD L^{-1} (Hanaki et al., 1981), 1-3 g COD L^{-1} (Ma et al., 2015) and 8.6-13 g COD L^{-1} (Dasa et al., 2016).The calibrated inhibition constants in this work fall in the same order of magnitude (see table 3). Consequently, methanogens were washed out from the bottom layer- $CSTR_1$ – by day 230, which is in agreement with the results obtained experimentally through Illumina sequencing by (Fernández-Palacios et al., 2021). A direct implication of this population switch is the growth of hydrogen-utilizing sulfate-reducers (X_{ASRB}) due to the sudden availability of H_2 – no longer consumed by X_{HM} in the NBP phase – as can be observed in figure 3.

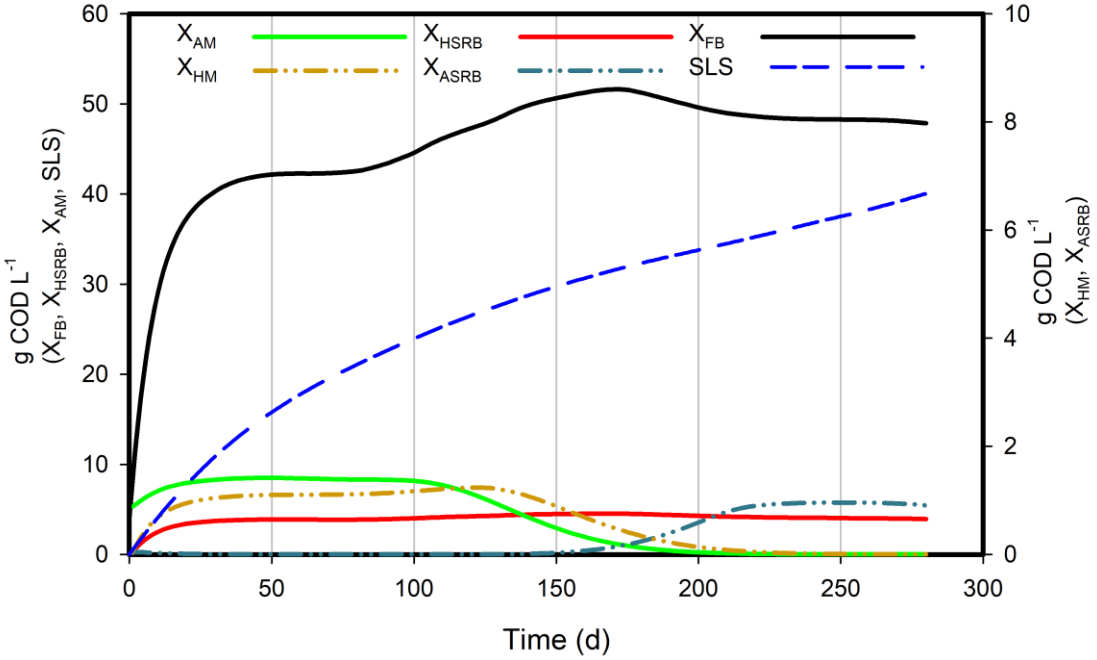

Fig. 3. Biomass dynamics in $CSTR_1$ predicted by the model. The profiles of acetoclastic and hydrogenotrophic methanogens (X_{AM} and X_{HM}), heterotrophic and autotrophic sulfate-reducers (X_{HSRB} and X_{ASRB}), fermenters (X_{FB}) and SLS during the 280 days of operation are shown.

Notably, a spike in fermentative bacteria growth is observed after 100 days of operation which is attributed to the pseudo steady-state feeding conditions of this experimental run, where the inlet concentration of glycerol was not constant in time but rather increased as the operation went through (see figure S2). This shift also explains the slight increase in SLS accumulation during the second half of the operation, as shown in figure 3.

Preferential pathways for glycerol fermentation, sulfate-reduction and methanogenesis

The average substrate consumption rates of the main biological processes considered in the model during both phases (BP and NBP) are shown in figure 4 (with values taken from table S9). As expected, the model predicted two main preferential pathways for glycerol fermentation; ethanol + formic acid production, accounting for 43%, and 1,3-propanediol production, accounting for 41%, which is in accordance with the reported mechanistic model (Zhou, Dorado, et al., 2022). (Sittijunda & Reungsang, 2017)also observed similar outcomes using both pure glycerol and crude glycerol in a UASB operating at different OLR. As a result, the main compounds utilized as electron donors for sulfate-reducing processes were ethanol and 1,3-propanediol, with a combined contribution of 72% during the NBP phase; these numbers are also in accordance with the results obtained by (Zhou et al., 2022), who observed a 78% in their batch activity tests.

373 Overall, a 20% increase in the sulfate-reducing capacity of the UASB was observed comparing the BP phase

374 with NBP phase, as also evidenced by the decrease in outlet sulfate concentration shown in figure 2B.

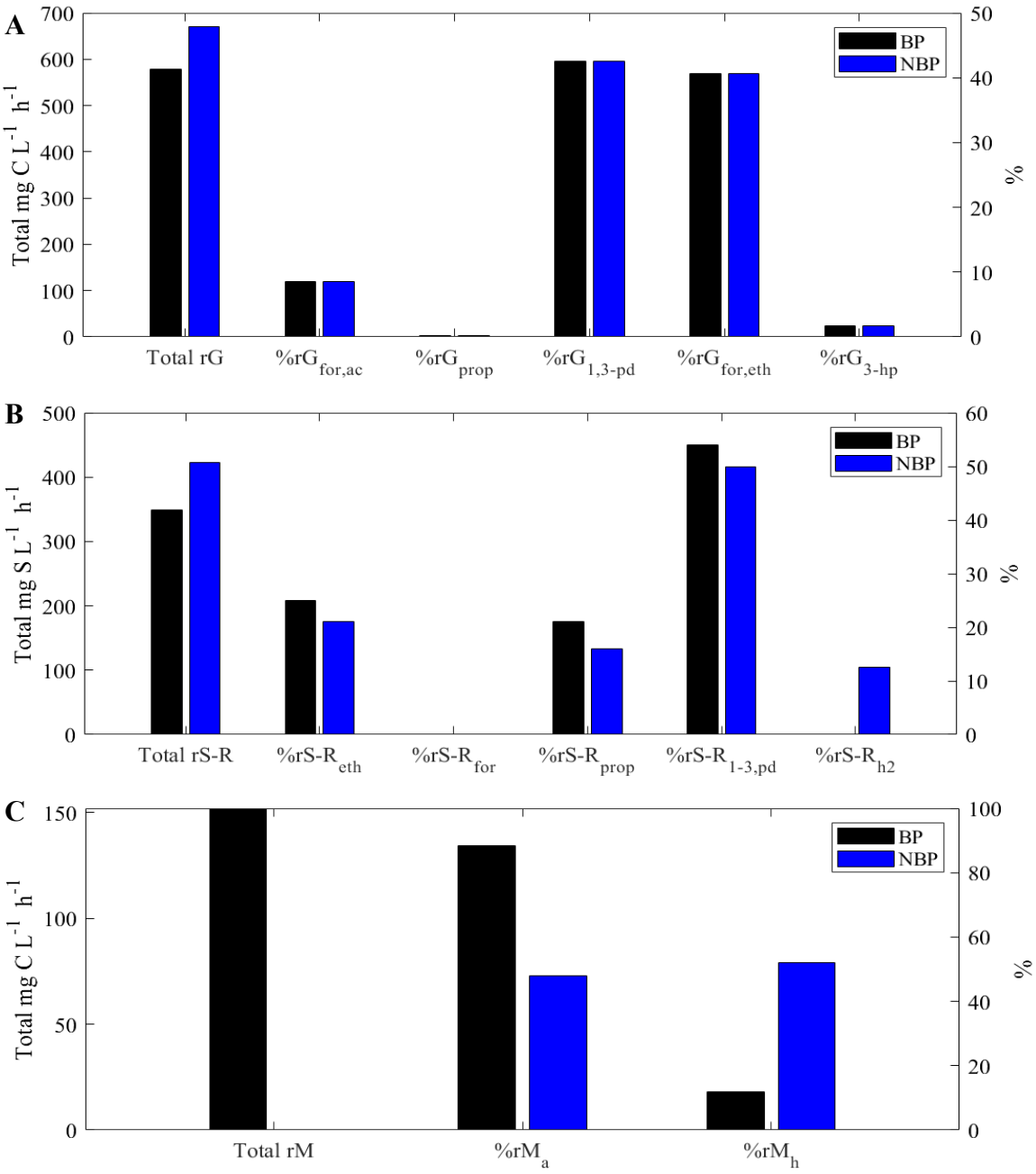

Fig. 4. Average biochemical rates, classified by 3 types of biological activity (A: glycerol fermentation, B: sulfate reduction, and C: methane production), during the biogas production and non-biogas production phases, in black and blue, respectively. For each biological activity, the total rate is shown – in mg L^{-1} h^{-1} – as well as the relative contributions of each pathway – in %. The data is shown and explained in table S9.

375 This increase can be attributed to 2 main reasons. Firstly, as previously noted, the increase in inlet glycerol

376 concentration led to a greater production of intermediates, thereby increasing the availability of electron donors

for sulfate reduction. Secondly, the emergence of H_2 – utilizing SRB (ASRB), which accounted for 13% of sulfate-reduction during the NBP phase.

However, the inhibitory effect caused by SLS have different effects on SR pathways; for instance, propionic uptake was slightly decreased whereas 1,3-propanediol uptake increased by 13% in the sulfate-reduction rate (see table S9).

Regarding methanogenic activity, the main pathway during the BP phase was the acetoclastic, accounting for 88% of methane production. Other studies have shown that the predominance of either pathway – acetoclastic or hydrogenotrophic – can depend on various factors such as the granule size (Owusu-Agyeman et al., 2019)or the presence of other acetate – consuming bacterial populations (Le et al., 2024). In this study the main causes for the acetoclastic pathway dominance were I) Low availability of hydrogen gas for X_{HM}, and II) Lack of competition for acetate. In fact, one of the singularities of the biological activity in this sulfidogenic UASB bioreactor was the inability to grow acetotrophic sulfate-reducing bacteria. This phenomenon was also observed in the previous experimental run of this system (Fernández-Palacios, 2019), which was used for model validation in this study. The authors suggested that the absence of these populations may have been due to growth limitations related to energetic considerations, i.e., their specific growth activity and biomass yield is lower when compared to other SRB populations. This fact supports the idea that the eventual washout of methanogenic populations was due to an inhibition process rather than substrate competition, as considered in other modelling studies (Kalyuzhny and Fedorovich, 1997; Sun et al., 2016; Chen et al., 2019).

3.3.Model validation

The validation of the model was conducted with data from (Palacios et al., 2019), as described in the methodology section, and the results are shown in figure 5.

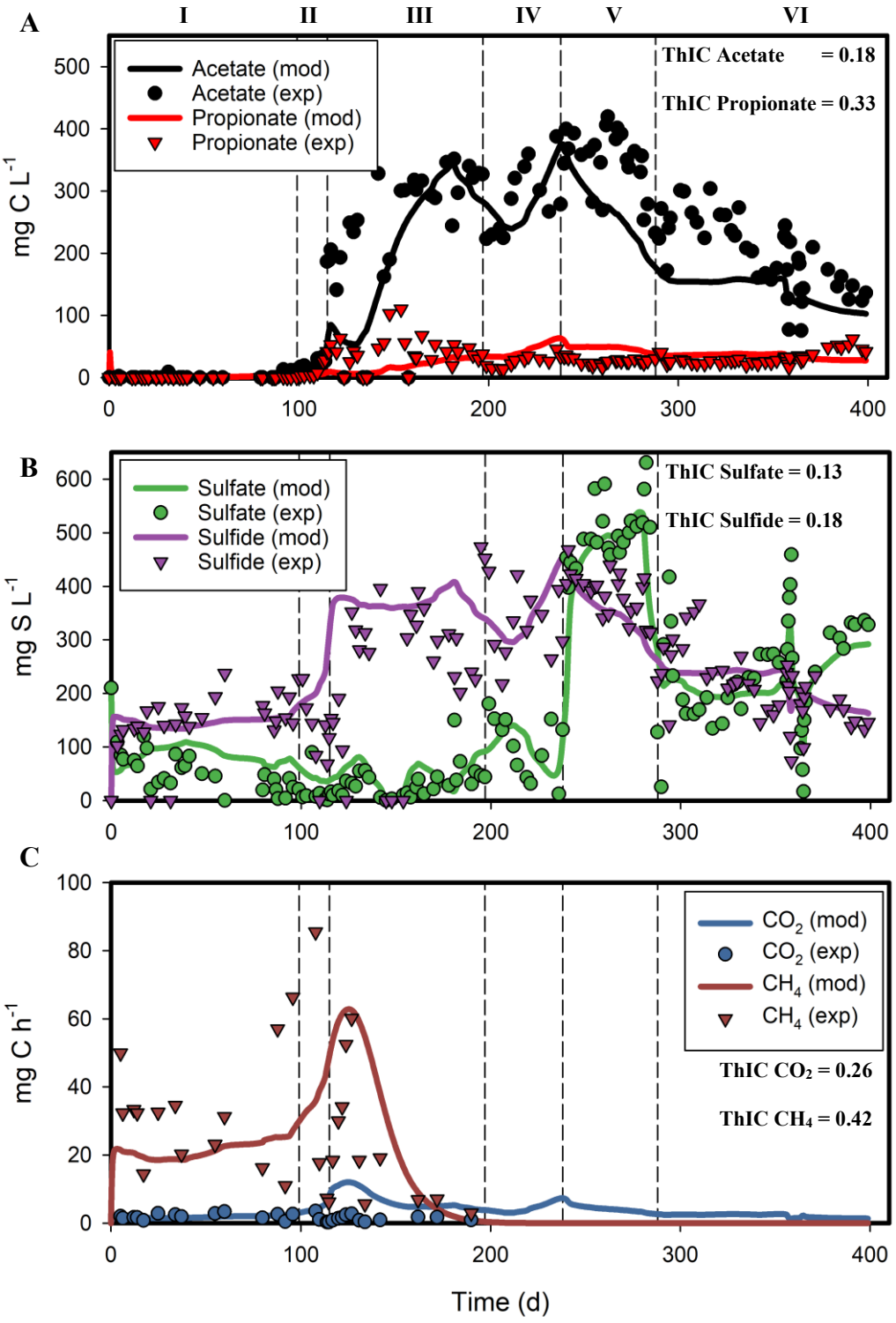

Fig. 5. Model validation results of: (A) acetate and propionate outlet concentrations, (B) sulfide and sulfate outlet concentrations and (C) methane and CO_2 outlet mass flowrates; the ThIC values for each fit are shown. The vertical dashed lines separate the 6 different experimental phases, the conditions of which can be found in table 1.

As can be observed, the model was able to predict the outcome of the main C and S species under 6 different experimental conditions, with changing inlet S and C loading rates and HRT as described in table 1. However, discrepancies between experimental data and model simulations were more pronounced compared to the calibration results shown in the previous section, especially in the cases of propionate and methane. One of the possible reasons for that is a more limited availability of data for this run – for instance regarding the inorganic carbon concentration in the inlet solution. Additionally, there is a slight delay in the loss of methanogenesis and the subsequent accumulation of VFAs, especially acetate. This delay suggests that a new pre-calibration procedure may be needed to accurately characterize the dynamics of the solids, which have an impact on the inhibition term (see equation 2). Noteworthy, the model demonstrates a rapid adaptation to changes in experimental conditions across the different phases, as evidenced by the sulfate and sulfide profiles. Additionally, the model accurately portrays the methanogenic endurance of the system, predicting its decline precisely at 200 days of operation.

Overall, these results demonstrate that the model is sufficiently reliable to predict the loss of methanogenic activity over time due to the accumulation of impurities coming from the glycerol solution. Therefore, the model can be utilized to predict the outcomes of this system under different conditions and scenarios, as will be detailed in the next section.

3.4.Scenario analysis

After calibrating and validating the mathematical model, a scenario analysis was conducted to evaluate the performance of the sulfidogenic UASB under different conditions. Since the model provided accurate predictions both with and without the inhibitory effect of SLS accumulation, two different case studies are investigated in this section: one using crude glycerol, where the impacts of the inhibitory effect will be assessed, and one using pure glycerine, where the overall performance of the system will be evaluated under different C and S loading rates.

Case study I

In the first case study, crude glycerol is set as the carbon source for the analyzed scenarios. The two variables of study are the concentration of SLS, represented as a % of the C, and time. Figure 6 shows the results of case study I.

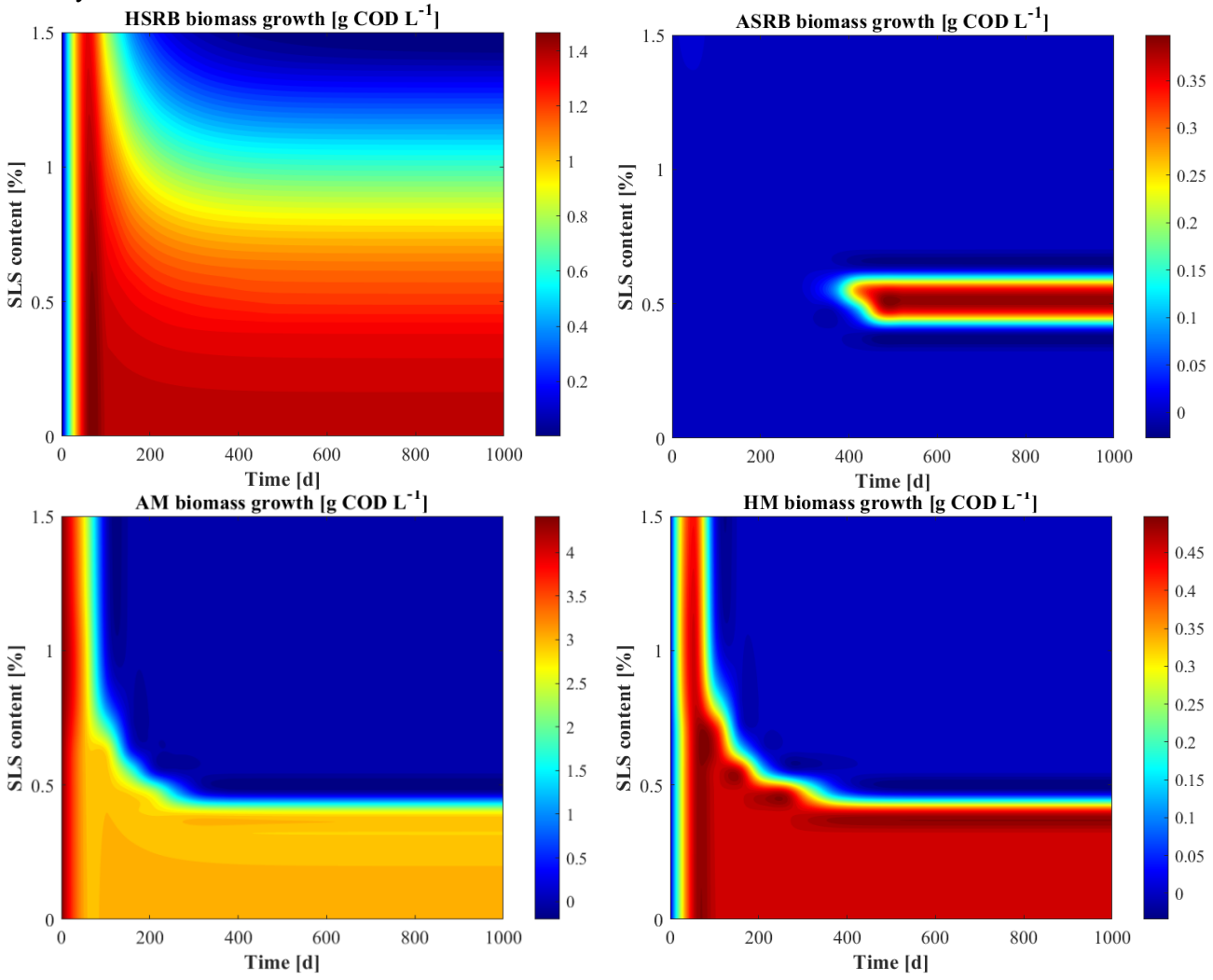

Fig. 6. Model scenario analysis, case study I. In the analyzed scenarios, the concentration of impurities in the inlet TOC solution ranges from 0 to1.5%, and the evolution of 4 different trophic groups (HSRB, ASRB, AM and HM) through 1000 days of operation at these different scenarios is shown.

464 The inhibitory effect of SLS on the different trophic groups can be easily observed by the limits where the
465 eventual wash-out of a given population occurs. Fermenters were left out of the study since this work is focused
466 on the inhibitory effect over sulfate-reducers and methanogens. Heterotrophic sulfate-reducers are the most
467 resilient faction, enduring SLS concentrations up to nearly 1.5%. Methanogens, however, are more sensitive,
468 with concentrations above 0.6% leading to their eventual washout (in this work, the calibrated value of SLS%
469 was of 0.63). Notably, the inhibition affects both methanogenic populations similarly, despite their differing
470 growth capacities. Interesting dynamics are observed with autotrophic sulfate-reducers, whose activity depends
471 on hydrogen availability; a strong inhibition of the hydrogenotrophic methanogenesis is, therefore, a necessary
472 condition for their long-term viability. This occurs at SLS concentrations between 0.4% and 0.6%, where the
473 inhibitory effect on hydrogenotrophic methanogens is strong enough to either cause their washout or
474 significantly reduce their hydrogen uptake. Within this range, ASRB populations emerge after 400 days of
475 operation and can be sustained in the long run. A more detailed picture of the biomass population profiles after
476 a given amount of time – in this case, 600 days – is provided in figure S3. These results portray, on a larger
477 scale, the interesting populational dynamics that may arise from the impact of inhibitory agents, in this case the
478 concentration of impurities (SLS).

479 Case study II

480 In the second case study, the aim was to assess the UASB performance in a context where its long-term operation
481 would not be hindered by any inhibitory agent, i.e., using a pure glycerin solution – free of impurities. In this
482 case the variables of study were the S and C loading rates, with the goal of covering a wide range of
483 combinations (from 0.1 to 27 g L^{-1} d^{-1}) that could offer different alternatives for real-scale applications. Figure
484 7 shows the results of biogas production rate, biogas purity – measured by % of methane –, sulfate removal
485 efficiency and effluent quality – measured by organic carbon content – after the system reaches a steady state
486 (70 days). As can be observed increasing the loading rates of C and S both result in a higher biogas production
487 rate, but the % of methane is equally hindered with these increases. This is primarily due to the mineralization
488 of organic carbon into CO_2, which significantly increases with higher C and S loads; the contribution of H_2S is
489 negligible in comparison.

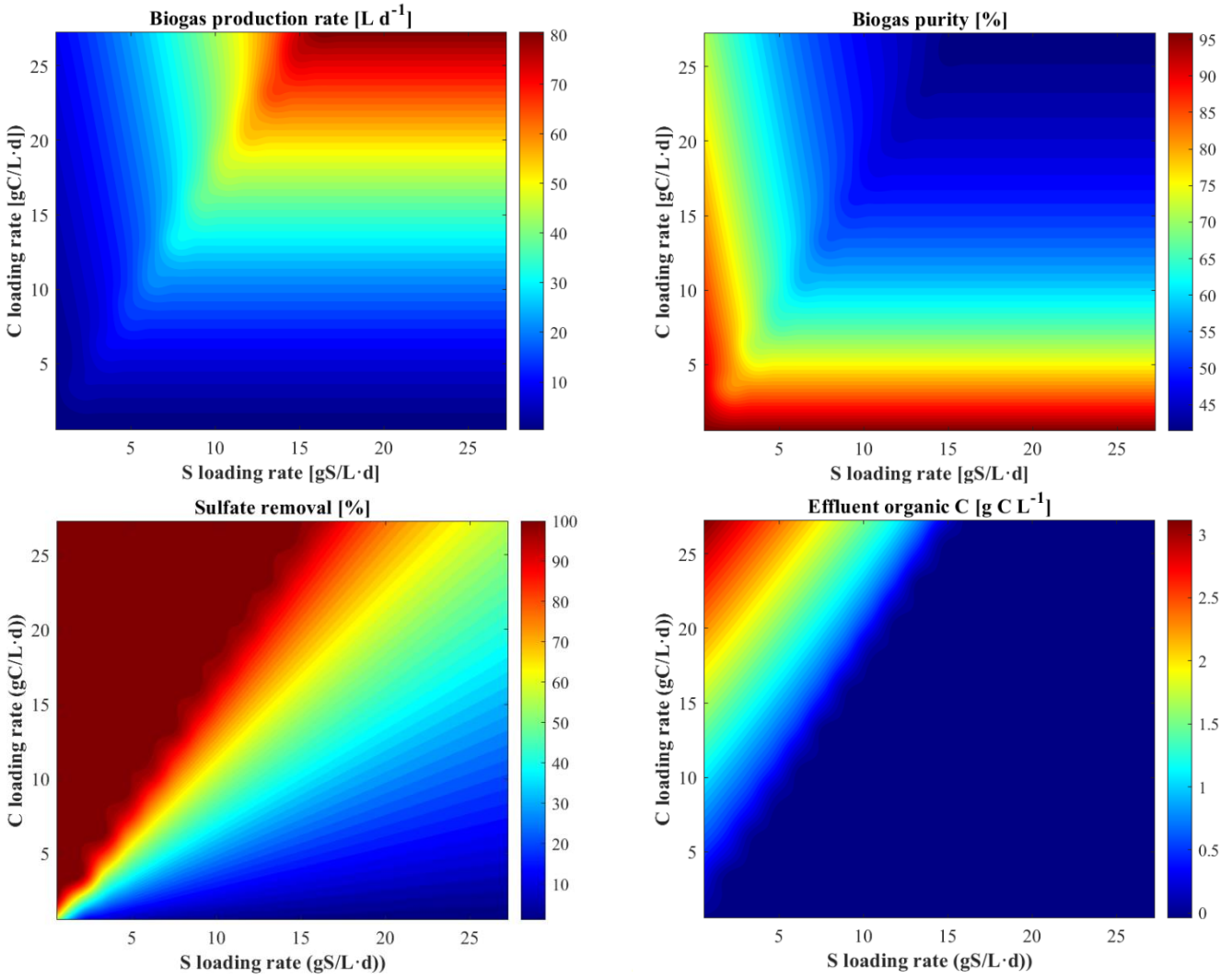

Fig. 7. Model scenario analysis, case study II. In the analysed scenarios, the inlet loading rates of C and S are varying within 0.1 and 27 g C/S L^{-1} d^{-1}. The biogas production rate [L d^{-1}], biogas purity (in CH_4 %), sulfate removal efficiency [%] and effluent organic carbon content [mg organic C L^{-1}] are shown as the output variables of interest.

In terms of effluent quality, a C/S ratio of 1.8 is needed to reduce all the sulfate into sulfide. (Sun et al., 2016) reported a lower C/S ratio of 0.6 g C g S^{-1} for complete sulfate reduction under steady-state conditions. This disparity may be attributed to the formation of fermentation intermediates from glycerol, such as 3-hydroxypropionate or acetate, which do not directly contribute to sulfate reduction in the present work.

However, achieving 100% sulfate removal efficiency results in a highly COD-loaded effluent, with concentrations ranging between 1-3 g C L^{-1} of organic compounds—mainly 1,3-propanediol, ethanol, and propionic acid. Therefore, operating at slightly lower C/S ratios is preferred; at a C/S of 1.6, effluent quality is significantly improved with minimal organic matter content, and a 90% sulfate removal efficiency is achieved. At this ratio, operating with higher loads will result into higher methane production rates, but at the same time

499 the purity of the biogas will be lower due to higher CO_2 and H_2S content. Therefore, the operational conditions
500 of a real-scale UASB would need to be set depending on many factors, such as the purity of glycerol fed or the
501 availability of an oxidizing unit to eliminate the remaining COD.

502

4. Conclusions

In this study, a comprehensive mathematical model describing the long-term operation of a sulfidogenic UASB bioreactor fed with crude glycerol has been developed, calibrated and validated successfully. The hydraulic model assumes a discretization into 3 mini-CSTRs, which allowed for the proper characterization of the transport of solids along the height of the reactor, including the impurities – SLS – coming from the crude glycerol solution. The biochemical model includes 15 biological processes carried out by 5 different trophic groups and incorporates the inhibitory effects of SLS over the microbial populations of the system.

Model calibration and validation followed a systematic approach using data from two independent experimental runs Calibration under pseudo steady-state feeding conditions accurately represented the transition between methanogenic and non-methanogenic conditions. The calibrated parameters were properly identifiable, and their estimated values were comparable with those found in other studies. An in-depth analysis of fermentation, sulfate reduction, and methanogenesis pathways showed general agreement with previous studies and highlighted the emergence of autotrophic SR during the non-biogas production phase. It is worth mentioning that the inhibition of the SLS over fermentative populations was not studied in this work and it could further improve the model predictions. Model validation under dynamic feeding conditions demonstrated the predictive capacity of the model as it was able to quickly adapt to the different experimental phases, and methanogenesis depletion was properly represented. However, a proper model pre-calibration could further increase the reliability of the model predictions, given the pivotal role of solids dynamics in this model formulation.

Finally, the validated model was used for scenario analysis with the aim of evaluating the UASB performance under different conditions with two case studies. In the first case study, the use of crude glycerol with varying SLS concentrations revealed distinct endurance of sulfate-reducers and methanogens over 1000 days of operation. The inhibitory impacts of SLS were found critical regarding hydrogen substrate competition between sulfate-reducers and methanogens. In the second case study, a wide range of C and S loading rates were investigated to assess the optimal conditions for UASB performance in terms of methane production and effluent quality. Higher organic matter and sulfate loads increased methane production but lowered biogas purity due to CO_2 production. A C/S ratio of 1.6 g C g S^{-1} was identified as optimal to improve the effluent quality.

This model can potentially be used for future studies of sulfidogenic UASB bioreactors operating with crude glycerol or glycerin as carbon source, either as a single-reactor model or as part of a multi-step process model for the removal or valorization of C and S from liquid effluents. Potential model improvements include the proper characterization of the long-term inhibition on fermentative populations and the description of the start-up phase of the operation.

Acknowledgements

This project has received funding from the European Union's Horizon 2020 research and innovation programme under the Marie Skłodowska-Curie grant agreement No. 872053.

References

Barrera, E. L., Spanjers, H., Solon, K., Amerlinck, Y., Nopens, I., & Dewulf, J. (2015). Modeling the anaerobic digestion of cane-molasses vinasse: Extension of the Anaerobic Digestion Model No. 1 (ADM1) with sulfate reduction for a very high strength and sulfate rich wastewater. *Water Research*, *71*, 42–54. https://doi.org/10.1016/j.watres.2014.12.026

Batstone, D. J., & Keller, J. (2003). Industrial applications of the IWA anaerobic digestion model No. 1 (ADM1). *Water Science and Technology : A Journal of the International Association on Water Pollution Research*, *47*(12), 199–206.

Batstone, D. J., Keller, J., Angelidaki, I., Kalyuzhnyi, S. V., Pavlostathis, S. G., Rozzi, A., Sanders, W. T. M., Siegrist, H., & Vavilin, V. A. (2002). The IWA Anaerobic Digestion Model No 1 (ADM1). *Water Science and Technology*, *45*(10), 65–73. https://doi.org/10.2166/wst.2002.0292

Boiocchi, R., Zhang, Q., Gao, M., & Liu, Y. (2022). Modeling and optimization of an upflow anaerobic sludge blanket (UASB) system treating blackwaters. *Journal of Environmental Chemical Engineering*, *10*(3). https://doi.org/10.1016/j.jece.2022.107614

Chen, H., Wu, J., Liu, B., Li, Y. you, & Yasui, H. (2019). Competitive dynamics of anaerobes during long-term biological sulfate reduction process in a UASB reactor. *Bioresource Technology*, *280*, 173–182. https://doi.org/10.1016/j.biortech.2019.02.023

Chen, J., Yan, S., Zhang, X., Tyagi, R. D., Surampalli, R. Y., & Valéro, J. R. (2018). Chemical and biological conversion of crude glycerol derived from waste cooking oil to biodiesel. *Waste Management*, *71*, 164–175. https://doi.org/10.1016/j.wasman.2017.10.044

Chen, R., Zhang, T., Guo, Y., Wang, J., Wei, J., & Yu, Q. (2021). Recent advances in simultaneous removal of SO2 and NOx from exhaust gases: Removal process, mechanism and kinetics. In *Chemical Engineering Journal* (Vol. 420). Elsevier B.V. https://doi.org/10.1016/j.cej.2020.127588

Chen, Y., He, J., Mu, Y., Huo, Y.-C., Zhang, Z., Kotsopoulos, T. A., & Zeng, R. J. (2015). Mathematical modeling of upflow anaerobic sludge blanket (UASB) reactors: Simultaneous accounting for

565 hydrodynamics and bio-dynamics. *Chemical Engineering Science*, *137*, 677–684.
566 https://doi.org/10.1016/j.ces.2015.07.016
567 Dasa, K. T., Westman, S. Y., Millati, R., Cahyanto, M. N., Taherzadeh, M. J., & Niklasson, C. (2016). Inhibitory
568 Effect of Long-Chain Fatty Acids on Biogas Production and the Protective Effect of Membrane Bioreactor.
569 *BioMed Research International*, *2016*, 1–9. https://doi.org/10.1155/2016/7263974
570 Deaver, J. A., Diviesti, K. I., Soni, M. N., Campbell, B. J., Finneran, K. T., & Popat, S. C. (2020). Palmitic acid
571 accumulation limits methane production in anaerobic co-digestion of fats, oils and grease with municipal
572 wastewater sludge. *Chemical Engineering Journal*, *396*. https://doi.org/10.1016/j.cej.2020.125235
573 Fedorovich & Kalyuzhnyi. (1997). Integrated mathematical model of uasb reactor for competition between
574 sulphate reduction and methanogenesis. *Water Science and Technology*, *36*(6–7).
575 https://doi.org/10.1016/S0273-1223(97)00524-6
576 Fernández-Palacios, E. (2020). *Integrated assessment of long-term sulfidogenesis in UASB reactors using crude*
577 *glycerol as carbon source*.
578 Fernández-Palacios, E., Lafuente, J., Mora, M., & Gabriel, D. (2019). Exploring the performance limits of a
579 sulfidogenic UASB during the long-term use of crude glycerol as electron donor. *Science of the Total*
580 *Environment*, *688*, 1184–1192. https://doi.org/10.1016/j.scitotenv.2019.06.371
581 Fernández-Palacios, E., Zhou, X., Mora, M., & Gabriel, D. (2021). Microbial diversity dynamics in a
582 methanogenic-sulfidogenic uasb reactor. *International Journal of Environmental Research and Public*
583 *Health*, *18*(3), 1–16. https://doi.org/10.3390/ijerph18031305
584 Flores-Alsina, X., Solon, K., Kazadi Mbamba, C., Tait, S., Gernaey, K. V., Jeppsson, U., & Batstone, D. J.
585 (2016). Modelling phosphorus (P), sulfur (S) and iron (Fe) interactions for dynamic simulations of
586 anaerobic digestion processes. *Water Research*, *95*, 370–382.
587 https://doi.org/10.1016/j.watres.2016.03.012
588 Guisasola, A., Baeza, J. A., Carrera, J., Sin, G., Vanrolleghem, P. A., & Lafuente, J. (2006). The Influence of
589 Experimental Data Quality and Quantity on Parameter Estimation Accuracy. Andrews Inhibition Model
590 as a Case Study. *Education for Chemical Engineers*, *1*(1), 139–145. https://doi.org/10.1205/ece06016

591 Hanaki, K., Matsuo, T., & Nagase, M. (1981). Mechanism of inhibition caused by long-chain fatty acids in
592 anaerobic digestion process. *Biotechnology and Bioengineering*, *23*(7), 1591–1610.
593 https://doi.org/10.1002/bit.260230717
594 Hu, S., Luo, X., Wan, C., & Li, Y. (2012). Characterization of crude glycerol from biodiesel plants. *Journal of*
595 *Agricultural and Food Chemistry*, *60*(23), 5915–5921. https://doi.org/10.1021/jf3008629
596 Huiliñir, C., Romero, R., Muñoz, C., Bornhardt, C., Roeckel, M., & Antileo, C. (2010). Dynamic modeling of
597 partial nitrification in a rotating disk biofilm reactor: Calibration, validation and simulation. *Biochemical*
598 *Engineering Journal*, *52*(1), 7–18. https://doi.org/10.1016/j.bej.2010.06.012
599 Jing, Z., Hu, Y., Niu, Q., Liu, Y., Li, Y. Y., & Wang, X. C. (2013). UASB performance and electron competition
600 between methane-producing archaea and sulfate-reducing bacteria in treating sulfate-rich wastewater
601 containing ethanol and acetate. *Bioresource Technology*, *137*, 349–357.
602 https://doi.org/10.1016/j.biortech.2013.03.137
603 Koster, I. W., & Cramert, A. (1987). Inhibition of Methanogenesis from Acetate in Granular Sludge by Long-
604 Chain Fatty Acids The effect of four saturated long-chain fatty acids (caprylic, capric, lauric, and myristic)
605 and one unsaturated long-chain fatty acid (oleic) on the microbial formation of methane from acetate was
606 investigated in batch anaerobic toxicity. In *APPLIED AND ENVIRONMENTAL MICROBIOLOGY*.
607 Le, T.-S., Bui, X.-T., Nguyen, P.-D., Hao Ngo, H., Dang, B.-T., Le Quang, D.-T., Thi Pham, T., Visvanathan,
608 C., & Diels, L. (2024). Bacterial community composition in a two-stage anaerobic membrane bioreactor
609 for co-digestion of food waste and food court wastewater. *Bioresource Technology*, *391*, 129925.
610 https://doi.org/10.1016/j.biortech.2023.129925
611 Li, Y., Jiang, J., Zhang, W., & Yang, G. (2023). Changes in stoichiometric ratio of carbon and sulfate affect
612 methanogenesis pathways in sulfate-rich sewers. *Journal of Cleaner Production*, *426*.
613 https://doi.org/10.1016/j.jclepro.2023.139112
614 Ma, J., Zhao, Q. B., Laurens, L. L. M., Jarvis, E. E., Nagle, N. J., Chen, S., & Frear, C. S. (2015). Mechanism,
615 kinetics and microbiology of inhibition caused by long-chain fatty acids in anaerobic digestion of algal
616 biomass. *Biotechnology for Biofuels*, *8*(1). https://doi.org/10.1186/s13068-015-0322-z

Mora, M., Fernández-Palacios, E., Guimerà, X., Lafuente, J., Gamisans, X., & Gabriel, D. (2020). Feasibility of S-rich streams valorization through a two-step biosulfur production process. *Chemosphere*, *253*. https://doi.org/10.1016/j.chemosphere.2020.126734

Nugroho, G., & Santoso, S. A. (2019). Dynamical modeling of substrate and biomass effluents in up-flow anaerobic sludge blanket (UASB) biogas reactor. *International Journal of Industrial Chemistry*, *10*(4), 311–319. https://doi.org/10.1007/s40090-019-00194-w

Owusu-Agyeman, I., Eyice, Ö., Cetecioglu, Z., & Plaza, E. (2019). The study of structure of anaerobic granules and methane producing pathways of pilot-scale UASB reactors treating municipal wastewater under sub-mesophilic conditions. *Bioresource Technology*, *290*, 121733. https://doi.org/10.1016/j.biortech.2019.121733

Pereira, M. A., Pires, O. C., Mota, M., & Alves, M. M. (2005). Anaerobic biodegradation of oleic and palmitic acids: Evidence of mass transfer limitations caused by long chain fatty acid accumulation onto the anaerobic sludge. *Biotechnology and Bioengineering*, *92*(1), 15–23. https://doi.org/10.1002/bit.20548

Rodríguez-Gómez, R., Renman, G., Moreno, L., & Liu, L. (2014). A model to describe the performance of the UASB reactor. *Biodegradation*, *25*(2), 239–251. https://doi.org/10.1007/s10532-013-9656-z

Rosén, C., Jeppsson, U., & Rosen, C. (2006). *Aspects on ADM1 Implementation within the BSM2 Framework*.

Silva, S. A., Salvador, A. F., Cavaleiro, A. J., Pereira, M. A., Stams, A. J. M., Alves, M. M., & Sousa, D. Z. (2016). Toxicity of long chain fatty acids towards acetate conversion by Methanosaeta concilii and Methanosarcina mazei. *Microbial Biotechnology*, *9*(4), 514–518. https://doi.org/10.1111/1751-7915.12365

Sittijunda, S., & Reungsang, A. (2017). Fermentation of hydrogen, 1,3-propanediol and ethanol from glycerol as affected by organic loading rate using up-flow anaerobic sludge blanket (UASB) reactor. *International Journal of Hydrogen Energy*, *42*(45), 27558–27569. https://doi.org/10.1016/j.ijhydene.2017.05.149

Smith, S. J., Pitcher, H., & Wigley, T. M. L. (2001). Global and regional anthropogenic sulfur dioxide emissions. In *Global and Planetary Change* (Vol. 29). www.elsevier.comrlocatergloplacha

Sun, J., Dai, X., Wang, Q., Pan, Y., & Ni, B. J. (2016). Modelling Methane Production and Sulfate Reduction in Anaerobic Granular Sludge Reactor with Ethanol as Electron Donor. *Scientific Reports*, *6*. https://doi.org/10.1038/srep35312

Valdés, E., Gabriel, D., González, D., Munz, G., & Polizzi, C. (2023). Integrating thermodynamics and mathematical modelling to investigate the stoichiometry and kinetics of sulphide oxidation-nitrate reduction with a special focus on partial autotrophic denitrification. *Chemosphere*, *339*. https://doi.org/10.1016/j.chemosphere.2023.139605

Viana, M. B., Freitas, A. V., Leitão, R. C., Pinto, G. A. S., & Santaella, S. T. (2012). Anaerobic digestion of crude glycerol: a review. *Environmental Technology Reviews*, *1*(1), 81–92. https://doi.org/10.1080/09593330.2012.692723

Wang, C., Shi, Q., Liu, L. F., Li, B., Li, Z., Hu, Y., Qi, W. K., Shen, W., Li, Y. Y., & Peng, Y. (2021). Mathematical modeling of methane production and sulfate reduction in upflow anaerobic sludge blanket reactors: Calibration, validation and prediction of reciprocal effects. *Environmental Technology and Innovation*, *24*. https://doi.org/10.1016/j.eti.2021.102014

Wu, J., Niu, Q., Li, L., Hu, Y., Mribet, C., Hojo, T., & Li, Y. Y. (2018). A gradual change between methanogenesis and sulfidogenesis during a long-term UASB treatment of sulfate-rich chemical wastewater. *Science of the Total Environment*, *636*, 168–176. https://doi.org/10.1016/j.scitotenv.2018.04.172

Wu, L. J., Kobayashi, T., Li, Y. Y., Xu, K. Q., & Lv, Y. (2017). Determination and abatement of methanogenic inhibition from oleic and palmitic acids. *International Biodeterioration and Biodegradation*, *123*, 10–16. https://doi.org/10.1016/j.ibiod.2017.05.021

Xianmin, Z. (1993). A New Method with High Confidence for Validation of Computer Simulation Models of Flight Systems. In *Chinese J. of Systems Engineering & Electronics* (Vol. 4, Issue 4).

Zeng, Y., Mu, S. J., Lou, S. J., Tartakovsky, B., Guiot, S. R., & Wu, P. (2005). Hydraulic modeling and axial dispersion analysis of UASB reactor. *Biochemical Engineering Journal*, *25*(2), 113–123. https://doi.org/10.1016/j.bej.2005.04.024

Zhou, X., Dorado, A. D., Lafuente, J., Gamisans, X., & Gabriel, D. (2022). Mechanistic modeling of glycerol fermenting and sulfate-reducing processes by granular sludge under sulfidogenic conditions. *Journal of Environmental Chemical Engineering*, *10*(3). https://doi.org/10.1016/j.jece.2022.107937

671 Zhou, X., Fernández-Palacios, E., Dorado, A. D., Gamisans, X., & Gabriel, D. (2022). Assessing main process
672 mechanism and rates of sulfate reduction by granular biomass fed with glycerol under sulfidogenic
673 conditions. *Chemosphere*, *286*. https://doi.org/10.1016/j.chemosphere.2021.131649
674 Zhou, X., Fernández-Palacios, E., Dorado, A. D., Lafuente, J., Gamisans, X., & Gabriel, D. (2024). The effect
675 of slime accumulated in a long-term operating UASB using crude glycerol to treat S-rich wastewater.
676 *Journal of Environmental Sciences (China)*, *135*, 353–366. https://doi.org/10.1016/j.jes.2022.11.011

677

678

Supplementary material

I. MATHEMATICAL MODEL FORMULATION

Table S1. Biochemical rate coeficients ($\nu_{i,j}$) of soluble components (i=1-12, j=1-15).

Table S2. Biochemical rate coeficients ($\nu_{i,j}$) of soluble and particulate components (i=12-24, j=16-30).

Table S3. Mass transfer rate coeficients ($\nu_{i,j}$) of soluble and gas components.

Table S4. Process mass transfer rate equations (ρ_j) of soluble and gas components.

Table S5. Process kinetic rate equations (r_j) of soluble components (j=1-15).

Table S6. Process kinetic rate equations (r_j) of soluble and particulate components (j=18-32).

Table S7. Kinetic, physical and chemical parameters of the mathematical model.

Table S1. Biochemical rate coefficients ($\nu_{i,j}$) of process rates (j=1-15) over soluble components (i=1-12).

Component *i*→		**1**	**2**	**3**	**4**	**5**	**6**	**7**	**8**	**9**	**10**	**11**	**12**
Process *j*↓		S_{for} [mg C L^{-1}]	S_{pro} [mg C L^{-1}]	S_{13PDO} [mg C L^{-1}]	S_{3HP} [mg C L^{-1}]	S_{eth} [mg C L^{-1}]	S_{ac} [mg C L^{-1}]	S_{H2} [mg H_2 L^{-1}]	S_{TIC} [mg C L^{-1}]	S_{CH4} [mg C L^{-1}]	$S_{sulfate}$ [mg S L^{-1}]	$S_{sulfide}$ [mg S L^{-1}]	S_{gly} [mg C L^{-1}]
1	Uptake of glycerol by FB	$\frac{(1-Y_{FB})}{3}$					$\frac{2\cdot(1-Y_{FB})}{3}$						-1
2	Uptake of glycerol by FB		$(1-Y_{FB})$										-1
3	Uptake of glycerol by FB			$(1-Y_{FB})$									-1
4	Uptake of glycerol by FB	$\frac{(1-Y_{FB})}{3}$				$\frac{2\cdot(1-Y_{FB})}{3}$							-1
5	Uptake of glycerol by FB				$(1-Y_{FB})$								-1
6	Uptake of formate by FB	-1						$\frac{(1-Y_{FB})}{6}$	$(1-Y_{FB})$				
7	Uptake of 3HP by FB (produce acetate)				-1		$\frac{2\cdot(1-Y_{FB})}{3}$		$\frac{(1-Y_{FB})}{3}$				
8	Uptake of 3HP by FB (produce propionate)		$(1-Y_{FB})$		-1								
9	Uptake of H_2 by ASRB							-1			$-4\cdot(1-Y_{ASRB})$	$4\cdot(1-Y_{ASRB})$	
10	Uptake of formate by HSRB	-1							$(1-Y_{HSRB})$		$\frac{-2\cdot(1-Y_{HSRB})}{3}$	$\frac{2\cdot(1-Y_{HSRB})}{3}$	
11	Uptake of propionate by HSRB		-1				$\frac{2\cdot(1-Y_{HSRB})}{3}$		$\frac{(1-Y_{HSRB})}{3}$		$\frac{-(1-Y_{HSRB})}{2}$	$\frac{(1-Y_{HSRB})}{2}$	
12	Uptake of ethanol by HSRB					-1	$(1-Y_{HSRB})$				$\frac{-2\cdot(1-Y_{HSRB})}{3}$	$\frac{2\cdot(1-Y_{HSRB})}{3}$	
13	Uptake of 1,3-propanediol by HSRB (produce 3HP)			-1	$(1-Y_{HSRB})$						$\frac{-8\cdot(1-Y_{HSRB})}{9}$	$\frac{8\cdot(1-Y_{HSRB})}{9}$	
14	Uptake of acetate by AM						-1		$\frac{(1-Y_{AM})}{2}$	$\frac{(1-Y_{AM})}{2}$			
15	Uptake of H2 by H2-M							-1	$\frac{-3\cdot(1-Y_{HM})}{2}$	$\frac{3\cdot(1-Y_{HM})}{2}$			

Table S2. Biochemical rate coeficients ($\nu_{i,j}$) of process rates (j=16-30) over soluble and particulate components (i=12-24).

Component *i*→		**12**	**13**	**14**	**15**	**16**	**17**	**18**	**19**	**20**	**21**	**22**	**23**	**24**
Process *j*↓		S_{gly} [mg C L^{-1}]	S_{CH} [mg COD L^{-1}]	S_{LI} [mg COD L^{-1}]	S_{IN} [mg COD L^{-1}]	S_{H+} [mol L^{-1}]	S_{OH-} [mol L^{-1}]	X_C [mg COD L^{-1}]	X_{IN} [mg COD L^{-1}]	X_{FB} [mg COD L^{-1}]	X_{ASRB} [mg COD L^{-1}]	X_{HSRB} [mg COD L^{-1}]	X_{HM} [mg COD L^{-1}]	X_{AM} [mg COD L^{-1}]
16	Growth of FB									1				
17	Growth of ASRB										1			
18	Growth of HSRB											1		
19	Growth of HM												1	
20	Growth of AM													1
21	Decay of FB							1		-1				
22	Decay of ASRB							1			-1			
23	Decay of HSRB							1				-1		
24	Decay of HM							1					-1	
25	Decay of AM							1						-1
26	Disintegration of composites		$1 \cdot f_{CH}$	$1 \cdot f_{LI}$	$1 \cdot f_{SI}$			-1	$1 \cdot f_{XI}$					
27	Hydrolysis of carbohydrates	$1 \cdot gly_{C/COD}$	-1											
28	Hydrolysis of lipids	$(1-ffa_{LI}) \cdot gly_{C/COD}$		-1										
29	Gain of H+					1								
30	Gain of OH-						1							

Table S3. Coefficients ($\nu_{i,j}$) of mass transfer process rates over soluble and gas components.

Process j ↓		Chemical states liquid phase				Chemical states gas phase [mol L^{-1}]			
		S_{H2} [mg H_2 L^{-1}]	S_{TIC} [mg C L^{-1}]	S_{CH4} [mg C L^{-1}]	$S_{sulfate}$ [mg S L^{-1}]	G_{H2}	G_{CO2}	G_{CH4}	G_{H2S}
1	H_2 stripping	-2000				1			
2	CO_2 stripping		-12000				1		
3	CH_4 stripping			-12000				1	
4	H_2S stripping				-32000				1

Table S4. Process mass transfer rate equations (ρ_j) of soluble and gas components.

j	**Process**	**Mass transfer rate expression** (ρ_j)	**Units**
1	H_2 stripping	$k_L a \cdot (\ S_{H2}/2000 - K_{H,H2} \cdot P_{H2})$	[mol L^{-1} h^{-1}]
2	CO_2 stripping	$k_L a \cdot (\ S_{CO2}/12000 - K_{H,CO2} \cdot P_{CO2})$	[mol L^{-1} h^{-1}]
3	CH_4 stripping	$k_L a \cdot (\ S_{\mathrm{CH4}}/12000 - K_{H,\mathrm{CH4}} \cdot P_{\mathrm{CH4}})$	[mol L^{-1} h^{-1}]
4	H_2S stripping	$k_L a \cdot (\ S_{sulfide}/32000 - K_{H,\mathrm{H2S}} \cdot P_{\mathrm{H2S}})$	[mol L^{-1} h^{-1}]

Table S5. Process kinetic rate equations (r_j) of soluble components (j=1-15).

j	Process	Kinetic rate expression (R_j)	Units
1	Uptake of glycerol by FB	$k_{m,gly1} \cdot \frac{S_{gly}}{k_{s,gly} + S_{gly}} \cdot I_{SLS,F} \cdot X_{FB}$	[mg C L^{-1} h^{-1}]
2	Uptake of glycerol by FB	$k_{m,gly2} \cdot \frac{S_{gly}}{k_{s,gly} + S_{gly}} \cdot I_{SLS,F} \cdot X_{FB}$	[mg C L^{-1} h^{-1}]
3	Uptake of glycerol by FB	$k_{m,gly3} \cdot \frac{S_{gly}}{k_{s,gly} + S_{gly}} \cdot I_{SLS,F} \cdot X_{FB}$	[mg C L^{-1} h^{-1}]
4	Uptake of glycerol by FB	$k_{m,gly4} \cdot \frac{S_{gly}}{k_{s,gly} + S_{gly}} \cdot I_{SLS,F} \cdot X_{FB}$	[mg C L^{-1} h^{-1}]
5	Uptake of glycerol by FB	$k_{m,gly5} \cdot \frac{S_{gly}}{k_{s,gly} + S_{gly}} \cdot I_{SLS,F} \cdot X_{FB}$	[mg C L^{-1} h^{-1}]
6	Uptake of formate by FB	$k_{m,for,F} \cdot \frac{S_{for}}{k_{s,for,FB} + S_{for}} \cdot I_{SLS,F} \cdot X_{FB}$	[mg C L^{-1} h^{-1}]
7	Uptake of 3HP by FB (produce acetate)	$k_{m,3hp1} \cdot \frac{S_{3HP}}{k_{s,3HP,FB} + S_{3HP}} \cdot I_{SLS,F} \cdot X_{FB}$	[mg C L^{-1} h^{-1}]
8	Uptake of 3HP by FB (produce propionate)	$k_{m,3hp2} \cdot \frac{S_{3HP}}{k_{s,3HP,FB} + S_{3HP}} \cdot I_{SLS,F} \cdot X_{FB}$	[mg C L^{-1} h^{-1}]
9	Uptake of H_2 by H2-SRB	$k_{m,ASRB} \cdot \frac{S_{H_2}}{k_{s,ASRB} + S_{H_2}} \cdot \frac{S_{SO4}}{k_{s,SO4} + S_{SO4}} \cdot I_{H_2S} \cdot I_{SLS,S} \cdot X_{ASRB}$	[mg H_2 L^{-1} h^{-1}]
10	Uptake of formate by HSRB	$k_{m,for,HSRB} \cdot \frac{S_{for}}{k_{s,for,HSRB} + S_{for}} \cdot \frac{S_{SO4}}{k_{s,SO4} + S_{SO4}} \cdot I_{H_2S} \cdot I_{SLS,S} \cdot X_{HSRB}$	[mg C L^{-1} h^{-1}]
11	Uptake of propionate by HSRB	$k_{m,pro} \cdot \frac{S_{pro}}{k_{s,pro,HSRB} + S_{pro}} \cdot \frac{S_{SO4}}{k_{s,SO4} + S_{SO4}} \cdot I_{H_2S} \cdot I_{SLS,S} \cdot X_{HSRB}$	[mg C L^{-1} h^{-1}]
12	Uptake of ethanol by HSRB	$k_{m,eth} \cdot \frac{S_{eth}}{k_{s,eth,HSRB} + S_{eth}} \cdot \frac{S_{SO4}}{k_{s,SO4} + S_{SO4}} \cdot I_{H_2S} \cdot I_{SLS,S} \cdot X_{HSRB}$	[mg C L^{-1} h^{-1}]
13	Uptake of 1,3-propanediol by HSRB (produce 3HP)	$k_{m,13PDO3} \cdot \frac{S_{13PDO}}{k_{s,13PDO3,HSRB} + S_{13PDO}} \cdot I_{H_2S} \cdot I_{SLS,S} \cdot X_{HSRB}$	[mg C L^{-1} h^{-1}]
14	Uptake of acetate by AM	$k_{m,AM} \cdot \frac{S_{ac}}{k_{s,ac} + S_{ac}} \cdot I_{SLS,M} \cdot X_{AM}$	[mg C L^{-1} h^{-1}]
15	Uptake of H2 by H2-M	$k_{m,HM} \cdot \frac{S_{H_2}}{k_{s,HM} + S_{H_2}} \cdot I_{SLS,M} \cdot X_{AM}$	[mg H_2 L^{-1} h^{-1}]

Inhibition factors:

$$I_{SLS,k} = \frac{ki_{SLS,k}\frac{X_k}{X_{SLS}}}{ki_{SLS,k}\frac{X_k}{X_{SLS}} + X_{SLS}}$$

Where $ki_{SLS,k}$ is the inhibition constant of SLS over trophic group k (mg COD_{SLS} L^{-1}) and X_{SLS} is the concentration of SLS (mg COD_{SLS} L^{-1}).

$$I_{H_2S} = \frac{1}{1 + \frac{S_{H_2S}}{ki_{H_2S}}}$$

Where ki_{H_2S} is the inhibition constant of S_{H_2S} over sulfate-reducing populations (ASRB and HSRB).

Table S6. Process kinetic rate equations (r_j) of soluble and particulate components (j=16-30).

j	Process	Kinetic rate expression (R_j)	Units
18	Growth of FB	$Y_{FB} \cdot \sum_{j=1}^{8} r_j$	[mg COD L^{-1} h^{-1}]
19	Growth of ASRB	$Y_{ASRB} \cdot r_9$	[mg COD L^{-1} h^{-1}]
20	Growth of HSRB	$Y_{HSRB} \cdot \sum_{j=10}^{13} r_j$	[mg COD L^{-1} h^{-1}]
21	Growth of HM	$Y_{HM} \cdot r_{14}$	[mg COD L^{-1} h^{-1}]
22	Growth of AM	$Y_{AM} \cdot r_{15}$	[mg COD L^{-1} h^{-1}]
23	Decay of FB	$k_d \cdot \mathrm{X_{FB}}$	[mg COD L^{-1} h^{-1}]
24	Decay of ASRB	$k_d \cdot \mathrm{X_{ASRB}}$	[mg COD L^{-1} h^{-1}]
25	Decay of HSRB	$k_d \cdot \mathrm{X_{HSRB}}$	[mg COD L^{-1} h^{-1}]
26	Decay of HM	$k_d \cdot \mathrm{X_{HM}}$	[mg COD L^{-1} h^{-1}]
27	Decay of AM	$k_d \cdot \mathrm{X_{AM}}$	[mg COD L^{-1} h^{-1}]
28	Disintegration of composites	$k_{dis} \cdot \mathrm{X_C}$	[mg COD L^{-1} h^{-1}]
29	Hydrolysis of carbohydrates	$k_{hyd,ch} \cdot \mathrm{X_{CH}}$	[mg C L^{-1} h^{-1}]
30	Hydrolysis of lipids	$k_{hyd,li} \cdot \mathrm{X_{LI}}$	[mg C L^{-1} h^{-1}]
31	Gain of H+	$\frac{2 \cdot r_1 + r_4 + r_5 + 2 \cdot r_7}{36000}$	[mol L^{-1} h^{-1}]
32	Gain of OH-	$\frac{r_3 + r_8}{36000} + \frac{r_9}{2000}$	[mol L^{-1} h^{-1}]

Table S7. Kinetic, physical and chemical parameters of the mathematical model (default values).

Cryptic Name	Variable Name	Value	Units
Y_{FB}	Yield of X_{FB}	0.132	[mg VSS mg C^{-1}]
Y_{HSRB}	Yield of X_{HRB}	0.077	[mg VSS mg C^{-1}]
Y_{ASRB}	Yield of X_{ASRB}	0.26	mg VSS mg H_2^{-1}
Y_{AM}	Yield of X_{AM}	0.087	[mg VSS mg C^{-1}]
Y_{HM}	Yield of X_{HM}	0.31	mg VSS mg H_2^{-1}
$k_{m,gly1}$	maximum specific uptake rate of glycerol by X_{FB} to produce acetate and formate	3.58	[mg C mg VSS^{-1} h^{-1}]
$k_{m,gly2}$	maximum specific uptake rate of glycerol by X_{FB} to produce propionate	0.1	[mg C mg VSS^{-1} h^{-1}]
$k_{m,gly3}$	maximum specific uptake rate of glycerol by X_{FB} to produce 1,3-propanediol	17.97	[mg C mg VSS^{-1} h^{-1}]
$k_{m,gly4}$	maximum specific uptake rate of glycerol by X_{FB} to produce formate and ethanol	17.13	[mg C mg VSS^{-1} h^{-1}]
$k_{m,gly5}$	maximum specific uptake rate of glycerol by X_{FB} to produce 3-hydroxypropionate	3.43	[mg C mg VSS^{-1} h^{-1}]
$k_{m,for,FB}$	maximum specific uptake rate of formate by X_{FB}	3.02	[mg C mg VSS^{-1} h^{-1}]
$k_{m,hp1}$	maximum specific uptake rate of 3-hydroxypropionate by X_{FB} to produce acetate	2.56	[mg C mg VSS^{-1} h^{-1}]
$k_{m,hp2}$	maximum specific uptake rate of 3-hydroxypropionate by X_{FB} to produce propionate	0.19	[mg C mg VSS^{-1} h^{-1}]
$k_{m,for,HSRB}$	maximum specific uptake rate of formate by X_{HSRB}	3.78	[mg C mg VSS^{-1} h^{-1}]
$k_{m,pro}$	maximum specific uptake rate of propionate by X_{HSRB}	9.96	[mg C mg VSS^{-1} h^{-1}]
$k_{m,pd}$	maximum specific uptake rate of 1,3-propanediol by X_{HSRB}	4.62	[mg C mg VSS^{-1} h^{-1}]
$k_{m,eth}$	maximum specific uptake rate of ethanol by X_{HSRB}	4.49	[mg C mg VSS^{-1} h^{-1}]
$k_{m,h2}$	maximum specific uptake rate of H_2 by X_{ASRB}	0.42	[mg H_2 mg VSS^{-1} h^{-1}]
$k_{m,am}$	maximum specific uptake rate of acetate by X_{AM}	1.25	[mg C mg VSS^{-1} h^{-1}]
$k_{m,hm}$	maximum specific uptake rate of H_2 by X_{HM}	0.24	[mg H_2 mg VSS^{-1} h^{-1}]
$k_{s,gly}$	half-saturation coefficient for the uptake of glycerol by X_{FB}	1.96	[mg C L^{-1}]
$k_{s,for,FB}$	half-saturation coefficient for the uptake of formate by X_{FB}	0.03	[mg C L^{-1}]
$k_{s,hp}$	half-saturation coefficient for the uptake of 3-hydroxypropionate by X_{FB}	6	[mg C L^{-1}]
$k_{s,for,HSRB}$	half-saturation coefficient for the uptake of formate by X_{HSRB}	53	[mg C L^{-1}]
$k_{s,pro}$	half-saturation coefficient for the uptake of propionate by X_{HSRB}	79	[mg C L^{-1}]
$k_{s,pd}$	half-saturation coefficient for the uptake of 1,3-propanediol by X_{HSRB}	45	[mg C L^{-1}]

$k_{s,eth}$	half-saturation coefficient for the uptake of ethanol by X_{HSRB}	45	[mg C L^{-1}]
$k_{s,h2}$	half-saturation coefficient for the uptake of H_2 by X_{ASRB}	0.0063	[mg H_2 L^{-1}]
$k_{s,am}$	half-saturation coefficient for the uptake of acetate by X_{AM}	47.85	[mg C L^{-1}]
$k_{s,hm}$	half-saturation coefficient for the uptake of H_2 by X_{HM}	8.7e-4	[mg H_2 L^{-1}]
$k_{s,so4,HSRB}$	half-saturation coefficient for the uptake of sulfate by X_{HSRB}	16.64	[mg S L^{-1}]
$k_{s,so4,ASRB}$	half-saturation coefficient for the uptake of sulfate by X_{ASRB}	1.344	[mg S L^{-1}]
k_d	decay rate for all trophic groups	0.48	[h^{-1}]
k_{dis}	desintegration rate of composites X_C	9.6	[h^{-1}]
$k_{hyd,ch}$	hydrolysys rate of carbohydrates S_{CH}	6	[h^{-1}]
$k_{hyd,lip}$	hydrolysys rate of lipids S_{LIP}	2.4	[h^{-1}]
$ki_{sls,F}$	inhibition constant of SLS over fermenters, X_{FB}	5e3	[mg COD L^{-1}]
$ki_{sls,SR}$	inhibition constant of SLS over sulfate-reducers, X_{HSRB} and X_{ASRB}	5e3	[mg COD L^{-1}]
$ki_{sls,M}$	inhibition constant of SLS over methanogens, X_{AM} and X_{HM}	5e3	[mg COD L^{-1}]
$ki_{h2s,SR}$	inhibition constant of free hydrogen sulfide over sulfate-reducers, X_{HSRB} and X_{ASRB}	250	[mg S L^{-1}]

II. MODEL SENSITIVITY ANALYSIS, CALIBRATION AND VALIDATION

The sensitivity (S_{ij}) of a parameter θ_i over a model output Y_j in time *t* was calculated according to Equation S1:

$$S_{j,t}(\theta_i) = \frac{Y_{j,t}(\theta_i+\Delta\theta_i)-Y_{j,t}(\theta_i-\Delta\theta_i)}{2\Delta\theta_i} \quad \text{Eq. (S1)}$$

Then, the cumulative sensitivity function through the operational time considered in this study (from t=0 to t=280 days) can be expressed as:

$$F_j(\theta_i) = \sum_{t0}^{t\,end} S_{j,t}(\theta_i) \quad \text{Eq. (S2)}$$

Finally, the relative sensitivity of a parameter θ_i over a model output Y_j can be expressed as:

$$RS_j(\theta_i) = 100 \cdot \frac{F_{j,max}(\theta_i)}{F_j(\theta_i)} \quad \text{Eq. (S3)}$$

Where $F_{j,max}$ is the cumulative sensitivity value of the most sensitive parameter over the analyzed output.

Table S8. Model sensitivity analysis of each kinetic parameter on propionate, acetate, methane, TIC, sulfate and sulfide outlets from the UASB. A disturbance factor of +-0.5 was applied to each parameter to test its local sensitivity to all variables. The relative sensitivity (%) of each variable to each parameter is shown, where 100% corresponds to the most sensitive parameter and the rest are calculated relative to it.

Parameter	Variables analysed						Average relative sensitivity
	Propionate	Acetate	Methane	TIC	Sulfate	Sulfide	
$km_{GF,for-ac}$	2.20	0.32	30.31	17.43	30.73	30.73	18.62
$km_{GF,prop}$	5.40	0.02	0.15	0.96	0.13	0.13	1.13
$km_{GF,1-3,pd}$	15.18	4.71	10000	31.96	100.00	100.00	58.64
$km_{GF,for-eth}$	28.61	4.55	84.92	21.91	37.01	37.01	35.67
$km_{GF,3hp}$	9.34	0.45	12.11	20.21	28.68	28.68	16.58
$km_{3HPF,for-ac}$	84.16	0.37	6.09	17.95	10.52	10.52	21.60
$km_{3HPF,for-prop}$	66.01	0.21	4.23	13.95	8.26	8.26	16.82
$km_{FOR,f}$	0.00	0.00	0.04	0.01	0.00	0.00	0.01
$km_{SR,h2}$	0.72	0.07	17.98	21.60	6.38	6.38	8.86
$km_{SR,for}$	0.00	0.00	0.00	0.01	0.00	0.00	0.00
$km_{SR,prop}$	100.00	0.35	3.83	9.82	0.80	0.80	19.27
$km_{SR,eth}$	6.26	5.56	53.58	66.50	9.76	9.76	25.24
$km_{SR,1,3-pd}$	12.43	6.47	22.62	49.54	7.54	7.54	17.69
$km_{M,ac}$	0.02	100.00	19.96	24.02	0.00	0.00	24.00
$km_{M,h2}$	1.22	0.14	74.28	100.00	26.46	26.46	38.09
ks_{GLY}	0.00	0.00	0.08	0.01	0.00	0.00	0.01
$ks_{FOR,f}$	0.00	0.00	9.51	0.01	0.00	0.00	1.59
ks_{PROP}	76.25	0.34	2.93	7.61	0.62	0.62	14.73
$ks_{FOR,sr}$	0.00	0.00	0.01	0.01	0.00	0.00	0.00
ks_{ETH}	3.49	4.42	30.96	38.33	5.60	5.60	14.73
$ks_{1,3-PD}$	6.29	3.62	9.40	20.92	3.15	3.15	7.76
$ks_{3HP,for-ac}$	65.47	0.29	4.24	13.92	8.18	8.18	16.72
$ks_{3HP,for-prop}$	82.32	0.27	5.96	17.54	10.39	10.39	21.14
$ks_{H2,sr}$	0.14	0.02	8.13	11.22	3.05	3.05	4.27
$ks_{SO4,hsr}$	0.07	0.01	9.00	2.28	0.66	0.66	2.11
$ks_{SO4,asr}$	0.85	0.09	18.16	0.82	0.12	0.12	3.36
$ks_{AC,m}$	0.01	53.90	10.73	12.95	0.00	0.00	12.93
$ks_{H2,m}$	0.10	0.01	5.33	7.42	2.00	2.00	2.81
$ki_{SLS,F}$	0.02	0.01	0.00	0.00	0.00	0.00	0.01
$ki_{SLS,M}$	0.02	7.85	2.92	1.52	0.49	0.49	2.21
$ki_{SLS,SR}$	2.16	0.80	0.73	1.78	0.28	0.28	1.00
k_{DIS}	0.01	0.03	0.01	0.04	0.00	0.00	0.02
$k_{HYD,CH}$	0.01	0.03	0.01	0.04	0.00	0.00	0.02
$k_{HYD,LIP}$	0.00	0.00	0.00	0.00	0.00	0.00	0.00
$ki_{H2S,SR}$	0.00	0.00	0.00	0.00	0.00	0.00	0.00

Table S9. Process rates after model calibration during biogas production phase (time = 50 days) and non-biogas production phase (time = 280 days). The absolute value of each sub-process rate is expressed, as well as the relative contribution of each sub-process to the overall process (%).

Process	Sub-process	Biogas production phase (days 0-100)			Non- Biogas production phase (days 230-280)		
		Rate [mg L^{-1} h^{-1}]	St. dev (±)	Relative contribution to process (%)	Rate [mg L^{-1} h^{-1}]	St. dev (±)	Relative contribution to process (%)
Glycerol fermentation [mg C L^{-1} h^{-1}]	rGF_{FOR-AC}	49.03	1,75	8.48	56.94	0,12	8.48
	rGF_{PROP}	1.37	0,05	0.24	1.59	0,00	0.24
	$rGF_{1.3-PD}$	246.12	8,77	42.57	285.79	0,62	42.57
	$rGF_{FOR-ETH}$	234.61	8,36	40.58	272.43	0,59	40.58
	rGF_{3HP}	46.98	1,67	8.13	54.55	0,12	8.13
3-HP fermentation [mg C L^{-1} h^{-1}]	$r3HP_{FOR-AC}$	57.57	1,81	24.58	62.52	0,64	24.58
	$r3HP_{FOR-PROP}$	176.67	5,54	75.42	191.87	1,95	75.42
Formic acid uptake [mg C L^{-1} h^{-1}]	rF_F	82.06	2,92	99.99	95.29	0,21	99.99
	[a] rF_{SR}	0.00	0,00	0.01	0.00	0,00	0.01
Sulfate reduction [mg S L^{-1} h^{-1}]	rSR_{ETH}	87.01	2,52	24.94	88.84	1,24	21.02
	[a] rSR_{FOR}	0.00	0,00	0.00	0.00	0,00	0.00
	rSR_{PROP}	73.51	1,97	21.08	67.97	1,70	16.08
	$rSR_{1.3-PD}$	188.14	6,34	53.93	212.47	0,92	50.29
	rSR_{H2}	0.16	0,45	0.05	53.26	1,42	12.60
Methanogenesis [mg C L^{-1} h^{-1}]	rM_A	133.93	3,15	88.30	0.07	0,07	47.79
	rM_H	17.75	0,74	11.70	0.06	0,06	52.21

[a] Both sub-processes refer to the same. In the first case the rate is expressed in mg C of formic acid uptaken per liter and hour, whereas in the second case it is expressed in mg S of sulfate reduced per liter and hour.

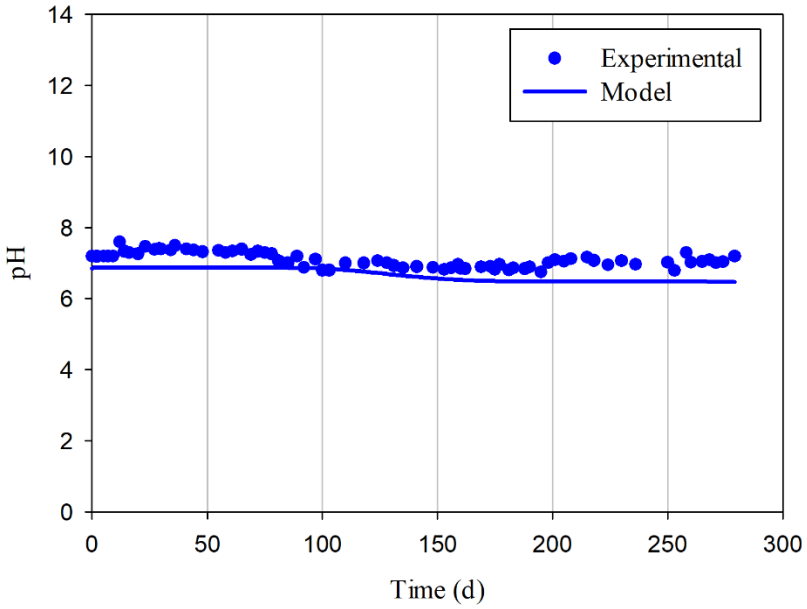

Fig. S1. Model predictions of the pH at the outlet of the UASB compared to the experimentally measured values. The ThIC value of the fit was 0.03.

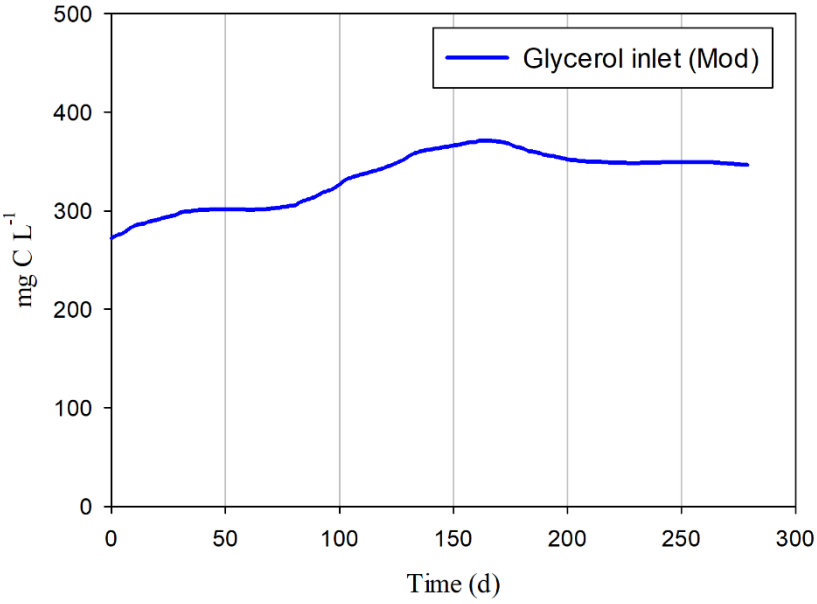

Fig. S2. Model input values of glycerol concentration in the inlet solution. These values are interpolated from the actual experimental values.

III. MODEL SCENARIO ANALYSIS

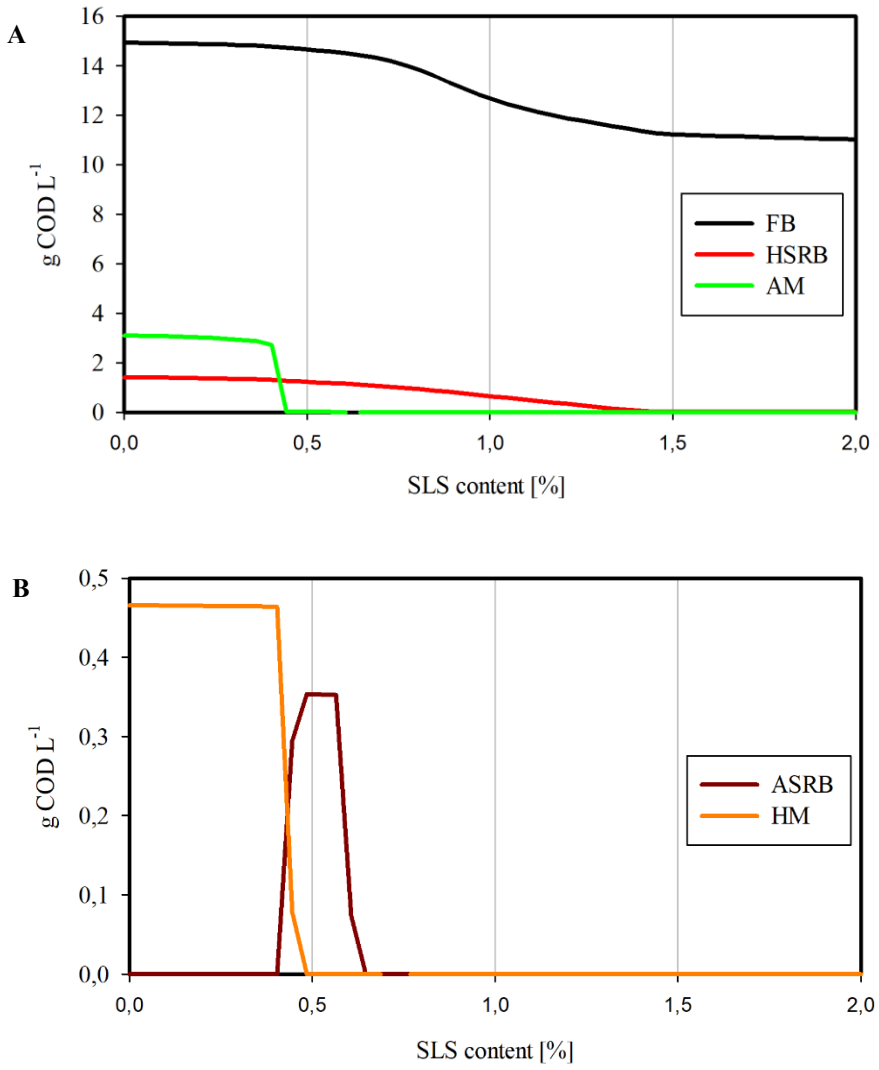

Fig. S3. Biomass growth of the 5 different trophic groups, after 600 days of operation, at different concentrations of impurities (SLS) in the TOC inlet solution. A) Fermentative bacteria (FB), heterotrophic sulfate-reducing bacteria (HSRB) and acetoclastic methanogens (AM); B) Autotrophic sulfate-reducing bacteria (ASRB) and hydrogenotrophic methanogens (HM).

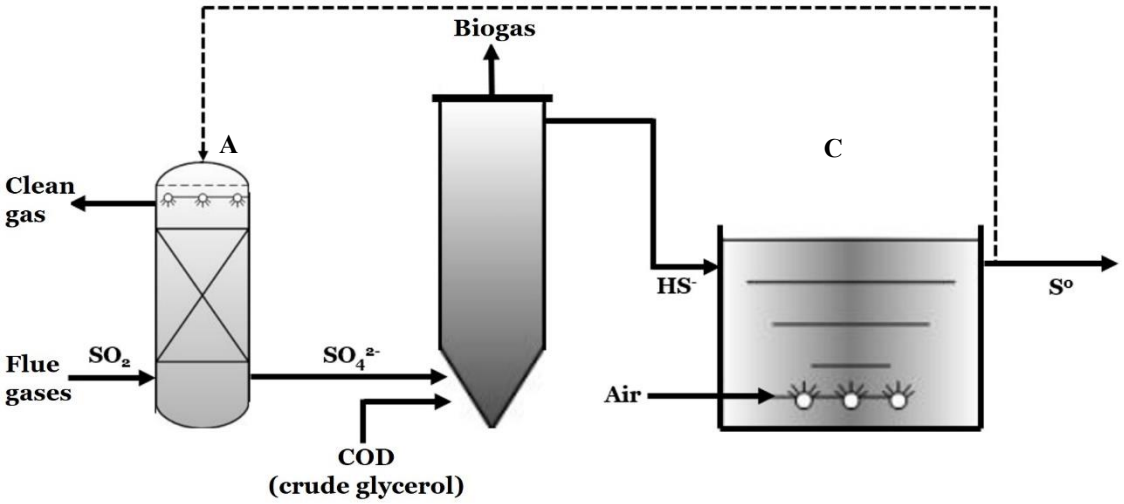

Fig. S4. Schematic representation of the SONOVA process (Mora et al., 2020). The process targets the revalorization of the S contained in the flue gases through a multi-step bioscrubber with an absorption column (A) and 2 biological stages: a sulfate-reducing UASB bioreactor (B) and an aerated sulfide – oxidizing CSTR. (C).